3D culture platform of human iPSCs-derived nociceptors for peripheral nerve modeling and tissue innervation

Biofabrication

PAPER

3D culture platform of human iPSCs-derived nociceptors for peripheral nerve modeling and tissue innervation

Afonso Malheiro[1,4], Abhishek Harichandan[1,4], Joyce Bernardi[2], Adrián Seijas-Gamardo[1], Gonda F Konings[3], Paul G A Volders[2], Andrea Romano[3], Carlos Mota[1], Paul Wieringa[1] and Lorenzo Moroni[1]

[1] MERLN Institute for Technology-Inspired Regenerative Medicine, Complex Tissue Regeneration department, Maastricht University, Maastricht, The Netherlands
[2] CARIM School for Cardiovascular Diseases, Department of Cardiology, Maastricht University, Maastricht, The Netherlands
[3] GROW School for Oncology and Developmental Biology, Department of Gynaecology, Maastricht University, Maastricht, The Netherlands
[4] These authors have contributed equally to this work.

E-mail: l.moroni@maastrichtuniversity.nl

Keywords: 3D, culture, human, iPSCs, nerve, innervation

Supplementary material for this article is available online

OPEN ACCESS

RECEIVED
11 May 2021

REVISED
1 November 2021

ACCEPTED FOR PUBLICATION
4 November 2021

PUBLISHED
30 November 2021

Abstract

Functional humanized *in vitro* nerve models are coveted as an alternative to animal models due to their ease of access, lower cost, clinical relevance and no need for recurrent animal sacrifice. To this end, we developed a sensory nerve model using induced pluripotent stem cells-derived nociceptors that are electrically active and exhibit a functional response to noxious stimuli. The differentiated neurons were co-cultured with primary Schwann cells on an aligned microfibrous scaffold to produce biomimetic peripheral nerve tissue. Compared to glass coverslips, our scaffold enhances tissue development and stabilization. Using this model, we demonstrate that myelin damage can be induced from hyperglycemia exposure (glucose at 45 mM) and mitigated by epalrestat (1 μM) supplementation. Through fibrin embedding of the platform, we were able to create 3D anisotropic myelinated tissue, reaching over 6.5 mm in length. Finally, as a proof-of-concept, we incorporated pancreatic pseudoislets and endometrial organoids into our nerve platform, to demonstrate the potential in generating nociceptor innervation models. In summary, we propose here an improved tool for neurobiology research with potential applications in pathology modeling, drug screening and target tissue innervation.

1. Introduction

The ability to detect external noxious stimuli and internal organ dysfunction signals is essential to maintain physical integrity and homeostasis [1]. This process is mediated by nociceptors, which recognize this input via specialized receptors, such as the transient receptor potential vanilloid 1 (TRPV-1), and conduct the information to the central nervous system (CNS), whilst also locally releasing neuropeptides, e.g. substance P, at the site of stimulus [2, 3]. The perception of nociceptive pain is contingent on the continuity of sensory peripheral nerve (PN) fibers between target organs and the CNS [4]. However, the PN is a fragile and exposed tissue, prone to damage by trauma or disease [5]. Most cases of PN damage arise from diabetes type II pathophysiological imbalances [6], which has prompted significant research into prevention and mitigation of diabetes-related disorders as well as strategies for neural tissue repair [7, 8]. In other pathological situations, the aberrant presence of nociceptors within organs can lead to abnormal and excessive pain. That is the case of chronic pancreatitis (CP), in which the main symptom is severe abdominal pain, caused in part by peripheral sensitization [9–11]. Similarly, women with endometriosis, a benign condition affecting up to 10% of reproductive-aged women, experience nociceptive pain because of infiltrating nociceptors within endometriotic implants and inflammatory sensitization of peripheral nociceptors [12].

To better understand PNs growth, repair methods and involvement in associated pathologies, it is necessary to develop improved neurobiology research platforms. Furthermore, such platforms

are instrumental in discovering compounds for neuropathy prevention, pain alleviation and nerve repair. To this end, biomimetic and functional three-dimensional (3D) *in vitro* models of PNs and tissue innervation can provide a simple, cost-effective and clinically relevant research tool to substitute the expensive and ethically loaded animal models. In this pursuit, few *in vitro* models using human sensory neurons and nociceptors in particular, have been reported. Wainger *et al* proposed a model using nociceptors from reprogrammed fibroblasts that were electrically active and sensitive to noxious stimuli [13]. Similarly, Jones *et al* [14] reported a sensory neuron model, with electrically excitable cells, obtained from human embryonic stem cell differentiation. Both models consist, however, of 2D disorganized and non-myelinated cultures, which do not reflect the biological architecture of mature nerves. To achieve myelination, Clark *et al* [15] generated co-cultures of induced pluripotent stem cells (iPSCs) derived sensory neurons with primary rat Schwann cells (SCs) on matrigel-coated coverslips. However, the use of matrigel limits clinical applicability (potential batch-to-batch variability) and the resultant tissue morphology is still flat and random. While 3D cultures exhibiting anisotropic neurites from iPSCs-derived motor neurons have already been reported for the creation of motor nerve [16] or innervated muscle platforms [17, 18], 3D biomimetic models with human functional sensory neurons are still limited.

We show here the development of a 3D sensory nerve model with biomimetic architecture and applicability for pathology modeling, drug testing and target tissue innervation. First, we developed a method to produce, in large-scale, uniform iPSCs-derived trunk neural crest (NC) spheroids (neurospheres) within an agarose mold. The neurospheres can be harvested from the mold and further differentiated into functional nociceptors that exhibit electrical activity and sensitivity to noxious stimuli (resininferatoxin, RTX). To develop a biomimetic nerve model, we co-cultured the neurospheres with primary rat SCs on an aligned microfibrous scaffold, which enhances neural tissue formation in terms of length, alignment and area, and improves tissue stabilization, compared to traditional glass coverslips. Using our 3D co-culture platform, we modeled diabetes-related myelin damage, through acute hyperglycemia exposure, and show that epalrestat is able to mitigate the damage. To upscale tissue formation, we combined the scaffold platform with a fibrin hydrogel, to create anisotropic myelinated axons, with over 6.5 mm in length, densely packed within a 3D matrix. Finally, using the biofabricated nerve platform, we incorporated pancreatic pseudoislets and endometrial organoids to demonstrate, as a proof-of-concept, the potential to generate various nociceptor-innervated models.

2. Materials and methods

2.1. Agarose microwell platform fabrication

A 3% (w/v) sterile agarose (Thermo Fisher Scientific) solution was prepared in phosphate buffered saline (PBS). Eight milliliter of agarose solution were poured onto an in-house fabricated Polydimethylsiloxane (PDMS) stamp with the negative template of 1580 microwells with 400 μm diameter. Centrifugation at 845 g was performed to remove air bubbles, followed by chilling for 45 min at 4 °C for agarose solidification. When solid, the agarose blocks were removed, cut to fit in a 12 well-plate, washed with 70% ethanol, then washed twice in PBS solution and left at 4 °C until further use. The day before cell seeding, PBS was replaced with Dulbecco´s Modified Eagel Medium (DMEM)/F-12 medium (Thermo Fisher Scientific) and kept in the incubator at 37 °C, 5% CO_2 overnight.

2.2. iPSCs culture

The human iPSC line LUMC0031iCTRL08 (Provided by the Leids Universitair Medisch Centrum iPSC core facility) was cultured on Geltrex coated dishes at a density of $10 \times 10^3\,cm^{-2}$ in mTESR1 medium (Stem Cell Technology). Cells were fed every day with completely fresh medium and passaged weekly using Gentle Cell Dissociation Reagent (Stemcell Technologies).

2.3. iPSCs differentiation into nociceptors and neurosphere formation

In order to induce iPSCs differentiation into nociceptors, we adapted and modified the protocol published by Chambers *et al* [19]. Nociceptor induction was initiated using single cell suspension of undifferentiated iPSCs detached with accutase, followed by seeding of 200 cells/microwell in mTESR1 medium supplemented with 10 μm of Y-27 632 and 0.5% Geltrex (in solution) onto 400 μm agarose microwells. Cell suspension was forced to settle by centrifugation at 290 g for 2 min. Afterwards, cells were incubated for 24 h and were given a complete media change with mTESR1 medium. At this time, the cellular spheroid is formed and cell synchronization is initiated by the addition of mTESR1 medium supplemented with 1% dimethyl sulfoxide (DMSO). The cells were maintained for 72 h in the synchronization medium. Post synchronization cells were given a PBS wash and nociceptor induction was initiated by addition of dual mothers against decapentaplegic (SMAD) inhibition media containing Advanced RPMI 1640 supplemented with Glutamax (both Thermo Fisher Scientific), 100 nM LDN-193 189 (Tocris) and 10 μM SB431542 (Tocris). The spheres were maintained for 48 h in the dual SMAD inhibition media. Following this, NC commitment was induced via media containing Advanced RPMI 1640 supplemented with Glutamax, 3 μM CHIR99021

(Tocris) and 1 μM retinoic acid (Tocris). The spheres were maintained in the NC induction media for 5 d with media change every alternate day. Following this stage, the spheres were incubated in notch inhibition media, consisting of Advanced RPMI supplemented with Glutamax, 10 μM SU5402 (Tocris) and 10 μM (2S)-N-[(3,5-Difluorophenyl)acetyl]-L-alanyl-2-phenyl]glycine 1,1-dimethylethyl ester (DAPT) (Tocris), for 48 h.

Finally, the neurospheres, composed of trunk NC cells, were collected and seeded on coverslips or scaffolds. In these substrates, cells were cultured in neural maturation medium for at least 5 d to reach the nociceptor phenotype. The neural medium is composed of Neurobasal Medium, 0.5 mM Glutamax, 100 U ml^{-1} penicillin and 100 μg ml^{-1} streptomycin (all Thermo Fisher Scientific), 100 ng ml^{-1} human nerve growth factor (NGF), 50 μg ml^{-1} ascorbic acid (all Sigma-Aldrich), 25 ng ml^{-1} human neuregulin-1 type III (NRG-1 sensory and motor neuron-derived factor (SMDF)) and N21 supplement (both from R&D systems).

2.4. Dissociated sensory neuron culture

iPSCs neurospheres were collected on day 9 of differentiation in an Eppendorf containing Advanced RPMI supplemented with Glutamax, and dissociated enzymatically with 1 ml of Trypsin Ethylenediaminetetraacetic acid (EDTA) for 10 min at 37 °C and 5% CO_2. Cells were pelleted at 1200 rpm for 7 min and resuspended in neural maturation medium, followed by mechanical dissociation though gentle repeated pipetting. The 5×10^3 cells cm^{-2} were seeded on matrigel coated (1:200 in DMEM) 35 mm petri dishes (for the patch clamp experiment) or 5×10^4 cells cm^{-2} on a six well plate (EIA experiment) and extra medium was added. The cultures were maintained in the same medium for up to 45 d, at 37 °C, 5% CO_2, with medium refreshment every 3 d. Cells probed for the conversion efficiency were let to attach for less than 24 h and then fixed.

2.5. Primary SCs harvesting, purification and culture

Primary SCs were harvested from the sciatic nerves of neonatal Wistar rat pups, following protocols compliant with the Dutch Animal Experimental Act and approved by the local ethical committee and national ethical authority, central committee for animal experiments. The license registration number 10 700 was used in communication with the Dutch authorities. The extraction and digestion of nerve segments and SC isolation and purification was conducted as previously described by us [20] and originally reported by Kaewkhaw *et al* [21].

2.6. Scaffold fabrication and sterilization

The scaffolds were fabricated via a two-step electrospinning process, using a custom-built apparatus, with ambient (temperature and humidity) control. In the first step, we produced a release layer by electrospraying a solution of 50% polyethyleneoxide (PEO, Mn = 3350, Sigma-Aldrich) in Milli-Q onto aluminum foil. The solution was flowed at 2 ml h^{-1} through a 0.8 mm inner diameter stainless steel needle (Unimed S.A.), while at 20 kV and at 10 cm from a rotating mandrel (60 mm diameter; 5000 rpm). Afterwards, we punched 12 mm circular holes on a nonwoven polyurethane mesh (6691 LL (40 g m^{-2}), a kind gift from Lantor B.V., the Netherlands), which was placed over the PEO-sprayed foil. The aligned scaffolds were produced via electrospinning of a Polybutylene terephthalate 300PEOT55PBT45 (PolyVation) in 75:25 chloroform/1,1,3,3-hexafluoroisopropanol solution over the mesh support structure. For this, the solution flowed at 0.75 ml h^{-1} through a 0.5 mm inner diameter stainless steel needle, while at 12 kV and at 10 cm from a rotating mandrel (at 5000 rpm). During both steps, the humidity was set at 35%–40% and the temperature at 22 °C–24 °C. Finally, individual scaffolds were obtained by punching a 15 mm-outer diameter sections concentric to the 12 mm holes, thus resulting in polyurethane mesh ring with spanning electrospun fibers. To detach the scaffolds from the aluminum foil, these were dipped in deionized water and left in PBS until further use. Prior to cell seeding, scaffolds were sterilized for 2 h in 70% ethanol, followed by air drying, several PBS washes and then maintained in PBS until further use.

2.7. Peripheral nerve (PN) platform generation

To fabricate our PN platform we followed the process graphically illustrated in figure 1. While the iPSCs differentiate and form neurospheres as described above, we simultaneously seeded the scaffolds with 100×10^3 primary SCs and cultured these for 7 d with SC medium (formulation described in Malheiro *et al* [20]). During this time, cells proliferated and aligned with the scaffold fibers to form highly anisotropic SCs bands within 7 days. At day 7, the SC medium was completely removed and 125 μl of neural medium was added. The neurospheres were transferred from the agarose mold to an Eppendorf containing 1 ml of neural medium and manually seeded onto the center of the scaffold (one neurosphere per scaffold). The scaffolds were transferred to a 24 well-plate and the neurospheres were let to adhere for 6 h at 37 °C, 5% CO_2. After this period, 0.75 ml of neural medium was added and an FKM O-ring (ERIKS) placed on top of the mesh ring to prevent scaffold floating.

For comparison, we also cultured neurospheres on scaffolds devoid of SCs, but with laminin coating, matrigel coating or no coating at all. For this, we incubated the scaffolds overnight with laminin solution: 100 μl of 1 μg ml^{-1} laminin-1 (R&D systems) and 2 μg ml^{-1} poly-D-lysine (Sigma Aldrich) in PBS; or matrigel solution: 100 μl of 1:200 dilution

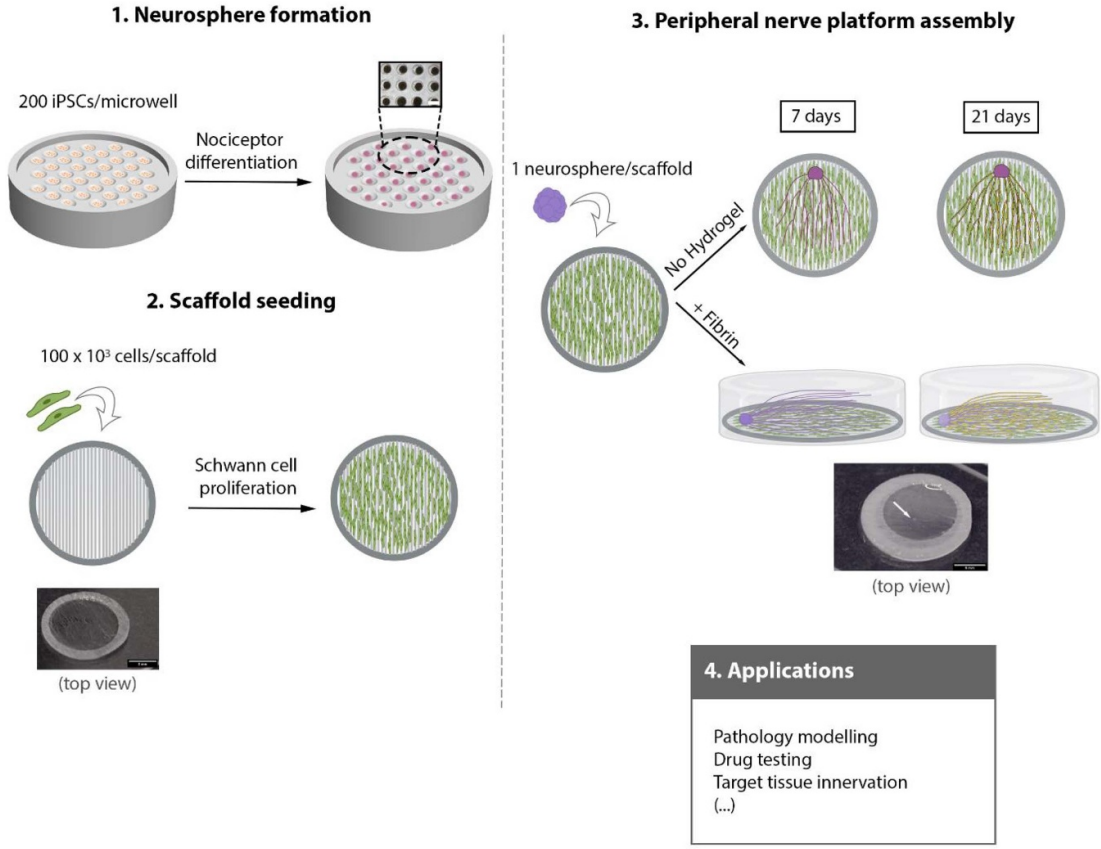

Figure 1. Illustration of the biofabrication steps to assemble our PN platform. (1) iPSCs differentiation into trunk NC cells and neurosphere formation (∼200 cells per sphere) in an agarose microwell platform (scale bar is 400 μm). (2) Scaffold seeding with primary rat SCs (100×10^3 cells) and formation of aligned SC bands after 7 days of culture; scale bar is 5 mm. (3) 3D PN platform assembly by neurosphere placement into the SC-seeded scaffold and co-cultured for 7 or 21 days, with or without a fibrin hydrogel embedding. Fibrin addition permits neural growth beyond the scaffold plane. Scale bar is 5 mm and the white arrow points to the neurosphere. (4) Overview of potential applications with this platform.

of matrigel stock (Fisher Scientific) in DMEM. The following day, we washed off the coating twice with sterile PBS and followed the same procedure for neurosphere seeding. All culture conditions were maintained for 7 or 21 days at 37 °C, 5% CO_2, with medium refreshment every other day.

2.8. Coverslip cultures

For sensory neuron marker characterization, we coated a 12 mm glass coverslip with laminin (same procedure as scaffold coating) and seeded one neurosphere as described above. The neurons were further cultured for 7 days with neural medium to induce maturation.

As a control for the scaffolds, we cultured neurospheres on bare (no coating), laminin, matrigel-coated or SCs-seeded 12 mm glass coverslips (same culture area as scaffolds). The laminin or matrigel coating procedure was identical to the scaffolds. SCs were seeded 7 days prior to neurosphere addition with the same cell density used for scaffold seeding (100×10^3 cells in total; $\sim 8.3 \times 10^3$ cells cm^{-2}). The cultures were maintained in neural medium for 7 or 21 days at 37 °C, 5% CO_2, with medium refreshment every other day.

2.9. Fibrin embedded PN platform

To produce a 3D biomimetic PN platform we combined a SCs-seeded scaffold with a neurosphere in a fibrin hydrogel. To achieve this, we followed a similar process as described above and illustrated in figure 1. First, 100×10^3 SCs were seeded on the scaffolds and induced to proliferate for 7 days. Thereafter, one neurosphere was seeded and the medium change to neural medium. After 1 day, we removed the medium and embedded the constructs into a fibrin hydrogel, composed of 3.5 mg ml^{-1} human fibrinogen (Enzyme Research Laboratories), 5 U ml^{-1} thrombin (Sigma-Aldrich) and 2.5 mM $CaCl_2$. After gelation (∼15 min), neural medium containing 100 μg ml^{-1} aprotinin was added. The cultures were maintained for 7 or 21 days at 37 °C, 5% CO_2, with medium refreshment every other day.

2.10. Pancreatic pseudoislets generation and innervation

To innervate pancreatic pseudoislets, we first generated spheroids composed of a mixture of alpha TC1 clone 6 cells (ATCC, CRL-2934) and INS1E cells (AddexBio), then added these onto a neurosphere seeded scaffold. To do this, we started

by expanding alpha TC cells in medium composed of DMEM, 15 mM (4-(2-hydroxyethyl)-1-piperazineethanesulfonic acid) (HEPES), 0.1 mM non-essential aminoacids, 2 g l^{-1} glucose (all Thermo Fisher Scientific), 10% FBS, 1.5 g l^{-1} sodium bicarbonate (both Sigma-Aldrich), 0.02% bovine serum albumin (BSA) (VWR) and INS1E cells in medium composed of Roswell Park Memorial Institute (RPMI), 2-mercaptoethanol, glutamax, HEPES, 100 U ml^{-1} penicillin and 100 μg ml^{-1} streptomycin (all Thermo Fisher Scientific) and 10% heat inactivated FBS (Sigma-Aldrich). When ready, the cells were seeded on a 200 μm agarose microwell platform at a ratio of 3:7 alpha TC/INS1E cells to yield approximately 250 cells per spheroid (protocol adapted from Hilderink *et al* [22]). The spheroids were cultured for 3 d in medium composed of 1:1 alpha TC/INS1E medium, then flushed from the platform and carefully pipetted onto a laminin-coated scaffold already containing one 7 d grown neurosphere. The spheroids were left to adhere overnight, after which we added 300 μl of fibrin hydrogel composed of 3.5 mg ml^{-1} human fibrinogen (Enzyme Research Laboratories), 5 U ml^{-1} thrombin (Sigma-Aldrich) and 2.5 mM $CaCl_2$. Cultures were maintained for 10 d with medium composed of 2:1:1 neural medium/alpha TC medium/INS1E medium at 37 °C, 5% CO_2.

2.11. Endometrium spheroids generation and innervation

The human endometrial adenocarcinoma cell line Ishi-M3-HSD-A is derived from Ishikawa cell line after genetic modification to introduce the luciferase fused with the green fluorescent reporters genes [23]. Cell line Ishi-M3-HSD-A used in the present experiment was authenticated by Short Tandem Repeat (AmpFlSTR IdentifilerTM PCR Amplification Kit; Thermo Fisher Scientific) profiling and tested negative for mycoplasma (MycoAlert, Promega).

Cells were maintained in standard monolayer culture as described earlier [23], using RPMI 1640 medium (Thermo Fisher Scientific) supplemented with sodium-pyruvate, L-glutamine, penicillin-streptomycin and 5% FBS at 37 °C with 5% CO_2 in humidified air. For organoid formation, cells were detached using with Accutase (Thermo Fisher Scientific), pelleted and resuspended in ice-cold matrigel (Becton Dickinson). Droplets of 25 μl matrigel suspension were pipetted into a 6 wells plate to form domes containing 2000 cells each. Matrigel domes were allowed to polymerize for 15 min at 37 °C, 5% CO_2 and were subsequently covered with pre-warmed endometrium organoid culture medium (RPMI 1640, sodium-pyruvate, L-glutamine, penicillin-streptomycin and 5% fetal bovine serum). Medium was refreshed twice a week, while monitoring the organoids condition.

For the innervation experiments, we carefully picked up the matrigel domes with a sterile spatula and transferred to a laminin-coated scaffold containing one 7 days grown neurosphere. The spheroids were left to adhere overnight, after which we added 300 μl of fibrin hydrogel composed of 3.5 mg ml^{-1} human fibrinogen (Enzyme Research Laboratories), 5 U ml^{-1} thrombin (Sigma-Aldrich) and 2.5 mM $CaCl_2$. Cultures were maintained for 10 d with medium of neural/endometrium at 1:1 ratio, containing 100 ng ml^{-1} NGF, at 37 °C, 5% CO_2.

2.12. Flow cytometry

iPSCs (100×10^3) were blocked for non-specific binding with 0.2 μg of polyglobin (Grifols) for 15 min at 4 °C, then incubated with the antibodies against human SSEA-3-AF647, SSEA-4-AF647, TRA 1–60-PE, TRA 1–81-PE (all from BD Biosciences) for 15 min at 4 °C. The cells were then washed twice in Fluorescence-activated Cell Sorting (FACS) buffer containing PBS supplemented with 0.1% bovine serum albumin (Sigma-Aldrich) and 0.0005% sodium azide (Sigma-Aldrich). The cells were further were incubated for 10 min at 4 °C with 1:1000 dilution of 1 mg ml^{-1} propidium iodide (PI) for the detection of dead cells. The cells were analyzed on a FACS Accuri flow cytometer analyzer (Becton Dickinson). The primary gating for selection of cells for analysis was done by selecting PI negative cells, which were further analyzed for the expression of the individual respective markers. The data acquired were analyzed using FlowJo software (FlowJo).

2.13. RNA extraction, reverse transcription, and quantitative RT-PCR

Harvested neural spheroids or cells were lysed in Trizol (ThermoFisher Scientific) and total Ribonucleic acid (RNA) was isolated using an RNeasy Mini Kit (QIAGEN). The RNA was reverse-transcribed with random primers and iScript™ cDNA Synthesis Kit (Invitrogen). Quantitative PCR was carried out using a Real-Time Polymerase chain reaction (PCR) System (Biorad) and iQ SYBR Green Supermix for qPCR (Biorad). Relative mRNA expression levels were analyzed by the $\Delta\Delta$CT method and normalized to Glyceraldehyde 3-phosphate dehydrogenase (GAPDH) gene expression. Three replicates were used per condition. Detailed primer information is provided in table S1 (available online at stacks.iop.org/BF/14/014105/mmedia).

2.14. Electrophysiology

Membrane potential of iPSC neurons of ~40 days post-differentiation was recorded in current-clamp mode. Action potentials (APs) were elicited by application of 200 pA current for 5 ms at a cycle length of 1 s. All measurements were performed in the

whole-cell configuration at physiological temperature (37 °C). Cells were superfused with an extracellular solution containing: 145 mM NaCl, 5.4 mM KCl, 1 mM $MgCl_2$, 10 mM HEPES, 1.8 mM $CaCl_2$, 10 mM glucose, adjusted at pH 7.4 with NaOH. Borosilicate glass pipettes were pulled (DMZ Universal Puller) at a resistance of 1.5–2.5 MΩ when filled with an internal solution containing: 110 mM KCl, 15 mM NaCl, 0.2 mM EGTA-KOH, 0.1 mM $CaCl_2$, 10 mM HEPES-KOH, 5 mM ATPMg^{2+}-salt, 10 mM glucose, adjusted at pH 7.2 with KOH. Membrane capacitance and series resistance were measured and compensated in every cell. Signals were acquired with an AxoPatch-1D amplifier (Axon Instrument), connected to a Digidata 1322 A (Axon Instrument) and sampled at 1 KHz after low-pass filtering at 10 KHz. Eight measurements were taken from a pool of four samples and the experiment repeated once. The final results were taken from an average of 8 measurements, displayed in table S2.

2.15. Quantification of substance P released from iPSCs-derived nociceptors after resiniferatoxin stimulation

Dissociated neurosphere cultures were prepared as described before and cultured for 10 days. Before changing the medium for the experiment, the cells were washed thoroughly with PBS. Then, 250 μl of control medium (normal neural medium), neural medium containing 100 nM RTX (Alomone Labs) or neural medium containing 100 mM potassium chloride (KCl) were added to the cultures. These were conditions incubated at 37 °C, 5% CO_2 for 5 min with gentle agitation. The supernatant was collected from each condition and immediately stored at −80 °C. To quantify the amount of substance P, we used the human substance P EIA kit (Phoenix PharmaceuticalsT, EK-061-05), and followed the manufacturer protocol. This experiment was performed once and five replicates per condition were used.

2.16. iPSCs-derived nociceptors morphology after resiniferatoxin and capsazepine (CPZ) stimulation

Neurospheres were seeded on laminin-coated coverslips as described above and cultured for 7 days. After this period, the culture medium was changed to control medium (normal neural medium), neural medium containing 1% ethanol (EtOH, vehicle control), neural medium containing 10 μM RTX or neural medium containing 10 μM RTX and 100 μM CPZ (Sigma-Aldrich) (both with 1% EtOH). To evaluate the neurite morphology, the initial 24 h of culture was tracked with brightfield microscopy and after this period the cells were fixed for subsequent immunostaining to βIII-tubulin. At $t = 24$ h cell viability was also quantified with the PrestoBlue™ Cell Viability Reagent (Thermo Fisher Scientific). Minimum of five replicates were used per condition.

2.17. Brightfield microscopy for live cells

To capture micrographs of live cells, we used the Nikon Eclipse TI-E microscope with an Okolabs environmental control. For the tracking of neurite morphology during the RTX/CPZ experiment, we transferred the coverslips containing the cell cultures to a 35 mm petri dish (Ibidi) and added control medium or medium supplemented with the drugs. The images were acquired immediately, taking frames every 5 min for 24 h.

2.18. Hyperglycemia test

The PN platform (without fibrin embedding) composed of SCs and one neurosphere was fabricated as described above and cultured for 21 days to allow mature myelin formation. At that point the medium was changed to either control medium (normal neural medium), hyperglycemic medium composed of normal medium supplemented with 45 mM glucose (Sigma-Aldrich, G7021) or hyperglycemic medium plus 1 μM epalrestat (Sigma-Aldrich, SML0527). Cultures were kept at 37 °C, 5% CO_2 for additional 48 h and then fixed with 4% paraformaldehyde (PFA) for 20 min at room temperature. Following this, the samples were prepared for immunostaining and transmission electron microscopy (TEM) as described below. Five replicates were used per condition.

2.19. Microscopy

Immunocytochemistry samples were fixed with 4% PFA for 20 min at room temperature (RT), rinsed thoroughly with PBS, and left in PBS until further use. Samples were permeabilized for 30 min at RT with 0.1% Triton X-100 in PBS, followed by rinsing with PBS and blocking with blocking buffer composed of 5% goat serum, 0.05% Tween-20, and 1% BSA in PBS, overnight at 4 °C, under mild agitation. Afterwards, samples were incubated overnight at 4 °C with primary antibody solutions in blocking buffer. The next day, the samples were washed with a wash buffer composed of 0.05% Tween20 and 1% BSA in PBS, and incubated for 2 h at RT with secondary antibody solutions in wash buffer. Following this, we rinsed the samples with PBS, stained with 4′,6-diamidino-2-phenylindole (DAPI) (0.2 μg ml^{-1}) for 10 min at RT, and left them in PBS until imaging. The detailed list of used primary and secondary antibodies can be found in tables S3 and S4 respectively. Images were acquired using either an inverted epifluorescence microscope coupled with a spinning disk (Nikon Eclipse Ti-e) or a confocal laser scanning microscope (Leica TCS SP8).

Samples for TEM were prepared as described in Malheiro *et al* [20]. After cutting, sections were stained with a toluidine blue solution (0.1% w/v in MiliQ water) for 1–2 min for histological evaluation of myelin presence (using a light microscope at 10 to 20X). Four sections, previously confirmed for myelin

presence, were taken from each biological sample and the same number of rings prepared. Finally, samples were imaged with FEI Tecnai G2 Spirit BioTWIN iCorr.

2.20. Image analysis

Three dimensional image reconstructions and neurite/myelin volume measurements were processed with Amira (Thermo Fisher Scientific). All other images were prepared and analyzed using Fiji software (https://fiji.sc/). To quantify the different parameters of tissue morphology, we obtained and analyzed images of the whole sample. To measure the orientation degree of fibers, neurites and myelin, we used the OrientationJ plugin [24] and applied the *Measure* function over circular ROIs that capture the whole tissue to obtain the coherence values (where 0 is full isotropy and 1 is full anisotropy). To measure the neurite length, we used the Simple Neurite Tracer plugin [25], and measured the distance between the cell bodies and the edge of the respective axons. Cell counts were performed using the standard *Analyze Particles* function to DAPI$^+$ objects. To measure the axonal area, we first converted images of βIII tubulin$^+$ cells to binary images and measured the pixel area occupied by the neurites, excluding cell bodies. Then, we divided this value by the total area of the scaffold. For the myelination area, we measured the pixel area of MBP$^+$ segments and divided this value by the area of the scaffold. *G*-ratio measurements were done using the *G*-ratio plugin (http://gratio.efil.de/) [26]. Myelin decompaction analysis was carried by first measuring the area below the most outer ring and the most inner ring (expected myelin area). Then, the image was converted to binary image and the same areas were determined (actual myelin area). To determine the decompaction area we used the following formula: (1 − (expected myelin area/actual myelin area)) × 100. For all experiments we used at least five biological replicates per condition. For the tissue morphological analysis (neurite alignment, axonal area and myelin area) we imaged and analyzed the whole sample. For neurite length quantification we took at least 15 measurements per sample. For myelin morphometric analysis (*g*-ratio and myelin decompaction) we took at least five measurements per sample.

2.21. Statistical analysis

The graphs were built and the data was analyzed using the software GraphPad Prism. Bar graphs are shown as mean ± SD and boxplots represent data points between the minimal and maximal value. Statistical significances were determined employing an unpaired *t*-test, one-way or two-way analysis of variance (ANOVA) followed by a Tukey's honestly significant difference (HSD) post-hoc test ($^*p < 0.05$, $^{**}p < 0.01$, $^{***}p < 0.005$, $^{****}p < 0.0001$ and ns is $p > 0.05$).

2.22. Illustrations

Illustrations were designed with either Adobe Illustrator CC 2018 (Adobe), SolidWorks (Dassault Systèmes) or with biorender (https://biorender.com/).

3. Results

3.1. Generation of human nociceptor neurospheres from iPSCs

To generate human nociceptor neurospheres we followed a two-step process detailed in figure 2(a). First, human iPSCs displaying a pluripotency phenotype (figure S1) were seeded on a 400 μm agarose microwell mold (200 cells/microwell; 1580 microwells) and the cells synchronized via DMSO treatment for 3 days. We then followed a differentiation protocol adapted from Chambers *et al* [19] in which human iPSCs were driven towards nociceptors, via a NC intermediate, in a quick and efficient manner. At day 2, and for 5 days, retinoic acid was supplemented together with CHIR99021 to promote cell aggregation. Retinoic acid supplementation is essential for the integrity of the spheroids, as its absence leads to poorly formed and loose clusters (figure S2(b)). At day 7, cells reached the NC stage denoted by the presence of SOX10$^+$ cells (figure S2(a)). To distinguish between cranial and trunk NC cells, we immunostained cells for ETS1, a cranial marker, and Phox2B, a trunk marker [27]. As shown in figure 2(b), most cells were Phox2B$^+$ rather than ETS1$^+$, evidencing commitment to the trunk phenotype. To confirm this, we also analyzed gene expression at different time points (figure 2(c)). At day 2, the expression of both markers was null. After 3 days, cells displayed a robust expression of ETS1, while Phox2B expression was still null. However, after 4 days of differentiation, we observed an inversion in marker expression, as cells exhibited an upregulation of Phox2B and downregulation of ETS1. Finally, at day 7 cells expressed only Phox2B, while ETS1 expression was null. At day 7 and for 2 days, we inhibited the notch signaling pathway through DAPT and SU5402 supplementation. At this stage, multiple uniform and cohesive spheroids (figures 2(d) and S2(c)) with an average diameter of 308.7 ± 38.6 μm were achieved. The conversion efficiency of this process up to this stage was measured via immunostaining to dissociated cells, revealing that 84.77% of these were positive for calcitonin-gene related peptide (CGRP) and 77.36% were positive to BRN3A (from the total cell count) (figure S3). For the second part of the process (at day 9 of differentiation), the neurospheres were harvested from the mold, seeded in a substrate of choice, and cultured with NGF-containing medium for at least 7 days, to finalize the nociceptor differentiation

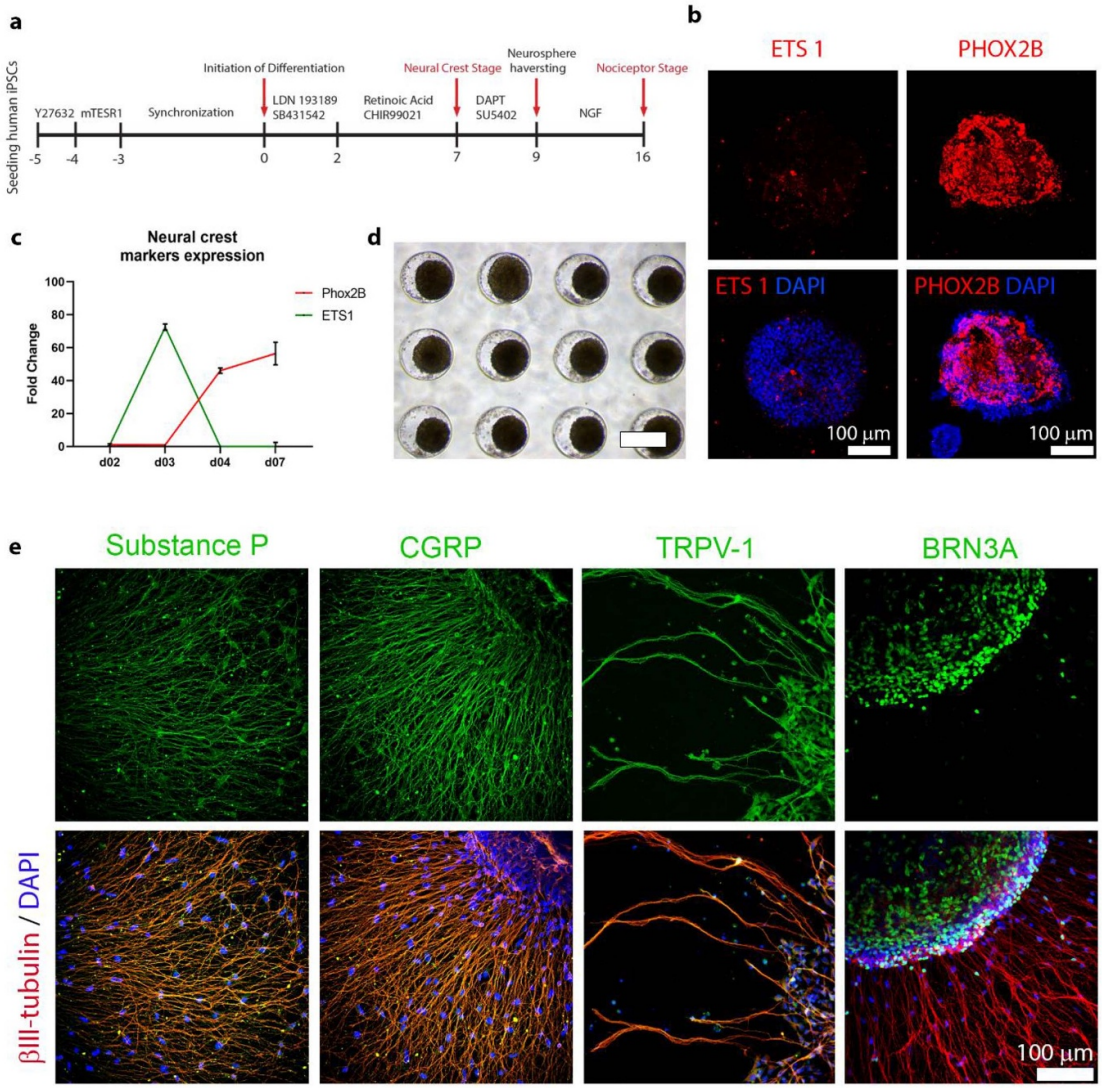

Figure 2. Differentiation process of iPSCs into nociceptor neurons. (A) Timeline of the protocol used to generate nociceptor spheroids from iPSCs cells. (B) Immunostaining of ETS1 (cranial marker; in red) or Phox2B (trunk marker; in red) on NC clusters (DAPI is shown in blue) (day 7 of differentiation). (C) Gene expression kinetics determined by quantitative Reverse transcription polymerase chain reaction (RT-PCR) analysis. Relative gene expression levels of transcripts to GAPDH expression at the indicated day point of differentiation of NC markers ETS1 (cranial) and Phox2B (trunk) ($n = 3$). (D) Brightfield micrograph of agarose microwells containing round and uniformly sized clusters with 308.7 ± 38.6 μm of diameter (scale bar is 400 μm). (E) Immunostaining to sensory neuron markers (in green)—substance P, CGRP, TRPV-1 and BRN3A—shows the successful differentiation of iPSCs into nociceptor neurons. Images are from neurospheres cultured for 7 days on laminin-coated coverslips. βIII-tubulin is shown in red and DAPI in blue.

protocol, whilst growing neurites *in situ*. To validate the acquisition of a nociceptor phenotype, we cultured the neurospheres on laminin-coated coverslips for 7 days and immunostained for the nociceptor-specific markers—substance P, CGRP and TRPV-1—and for the sensory neuron transcription factor—BRN3A. As shown in figure 2(e), all markers were expressed within grown neurons and located either along the length of the axons (substance P, CGRP and TRPV-1 correlated with βIII-tubulin) or in the nucleus (BRN3A correlated with DAPI). A comparison with primary nociceptors from rat dorsal root ganglion (DRG) neurons is provided in figure S4. In sum, we were able to generate a large number of even-sized nociceptor neurospheres in simple and quick manner.

3.2. Neuron function testing on nociceptor neurospheres

Nociceptor neurospheres were either dissociated to single cells (figures 3(a)–(c)) or kept intact (figures 3(d)–(g)) in order to validate neuron function, i.e. electrical excitability, and nociceptor function in particular, i.e. responsiveness to noxious stimuli. Whole-cell patch clamp measurements to dissociated neurons showed a mean membrane capacitance of 16.2 ± 4.2 pF, a mean resting membrane potential (RMP) of −44.1 ± 7.1 mV. All probed neurons were excitable and able to fire APs with a mean AP amplitude of 67.4 ± 26.2 mV and an overshoot peak of 23.3 ± 28.5 mV ($n = 8$) (figure 3(b)). To probe sensitivity to noxious stimuli, we measured

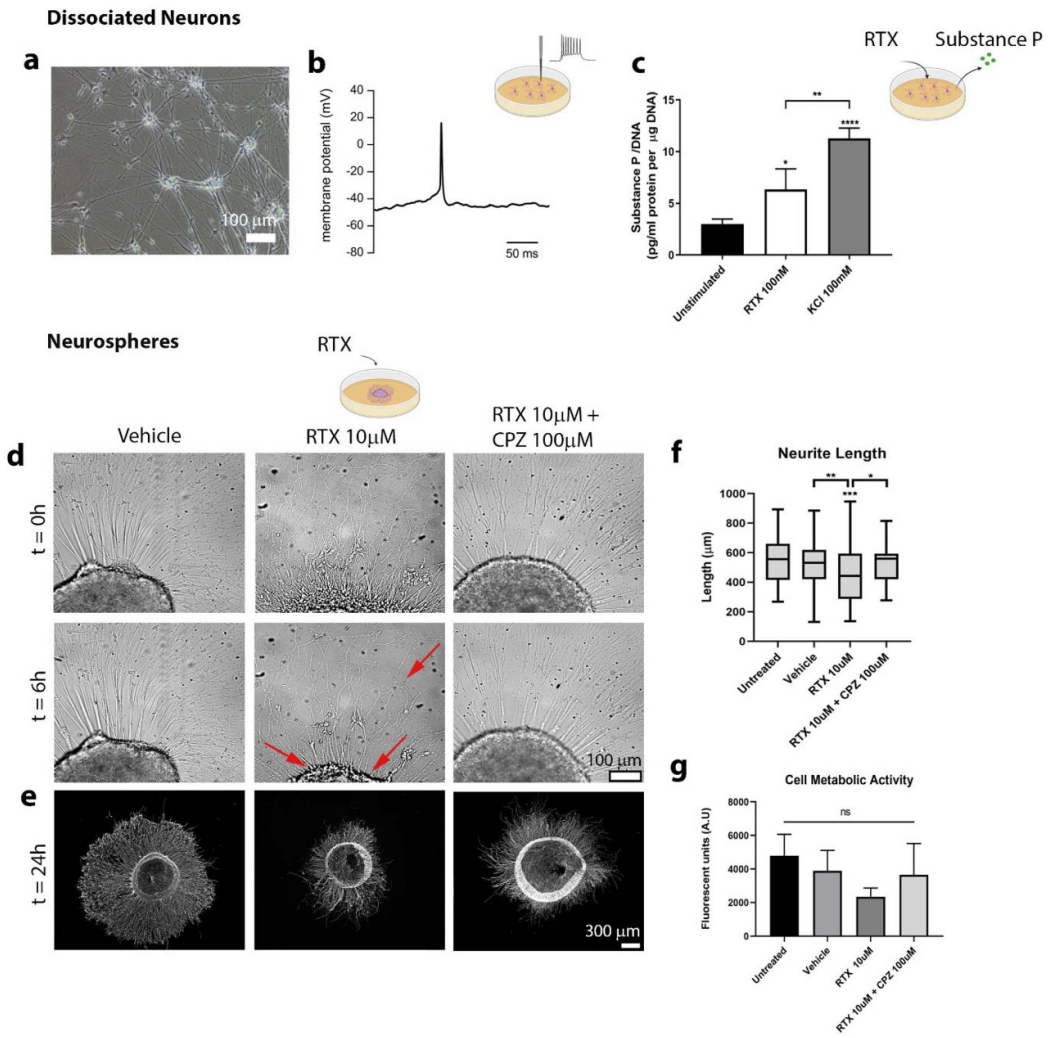

Figure 3. Neuron function tests on iPSCs-derived nociceptors. Top panel (A)–(C): tests on dissociated neurons. Bottom panel (D)–(G): tests on neurospheres. (A) Brightfield micrograph of ∼40 d old dissociated neurons. (B) Representative AP recorded from the neurons in response to 200 pA current injection for 5 ms. The mean RMP was −44.1 mV and the mean overshoot was 23.3 mV. (C) Release of substance P in response to a noxious stimulus (RTX; white bars) from 10 days old nociceptors. Untreated cells (black bars) and KCl-stimulated cells (gray bars) were used as controls. Graphical representation of the released substance P (in pg) relative to Deoxyribonucleic acid (DNA) amount (in μg). (D), (E) Stimulation of nociceptor neurospheres with RTX 10 μM or RTX 10 μM plus CPZ 100 μM. Untreated (normal neural medium) or vehicle (neural medium with 1% EtOH) were used as controls. (D) Live cell brightfield frames at $t = 0$ h or $t = 6$ h. The red arrows point to areas were neurite retraction overtime is visible (scale bar is 100 μm). (E) Immunostaining to βIII-tubulin of samples fixed 24 h after drug exposure. (F) Corresponding neurite length measurements (15 measurements per sample) and (G) cell metabolic activity (in arbitrary units) of samples 24 h after drug exposure. For (D) and (E) note that untreated cultures are not shown. All experiments were performed once and a minimum of five replicates were used per condition. The boxplots in (F) represent data points from the minimum to maximum value. All graph bars are represented as mean value ± SD and the statistics were performed with one-way ANOVA followed by a Tukey's HSD post-hoc test, where $^{****}p < 0.0001$, $^{***}p < 0.001$, $^{**}p < 0.01$, $^{*}p < 0.05$ and ns denotes $p > 0.05$.

the secretion of substance P after stimulation with RTX, a TRPV-1 agonist and analog of capsaicin [28]. As exhibited in figure 3(c), RTX exposure led to an immediate release of substance P from the nociceptor population. Specifically, RTX-stimulated neurons displayed a 2.12-fold increase of released substance P per DNA ($p < 0.05$) compared to unstimulated neurons. KCl-depolarized neurons showed an increment of 1.6 times compared to RTX-stimulated neurons ($p < 0.01$) and 3.8 times compared to unstimulated cells ($p < 0.0001$). Literature reports have shown that capsaicin exposure can lead to nerve fiber retraction and local denervation, after topical application of capsaicin on the skin [29]. Because of this, we explored if RTX exposure would lead to neurite retraction and if that effect could be mitigated by blocking the TRPV-1 channel with the antagonist CPZ [28]. To this end, the neurite morphology of nociceptor neurospheres was monitored for 24 h after the application of RTX alone or with RTX together with CPZ and compared with unstimulated cells or cells stimulated with vehicle medium (neural medium with 1% EtOH). As visible in figure 3(d), the neurites of neurospheres stimulated with vehicle (figure 3(d) left column and movie S1) or RTX plus CPZ (figure 3(d) right column and

movie S3) remained unaffected and showed little movement, except for the natural movement of live neurons. Contrarily, when stimulated with RTX only (figure 3(d) middle column and movie S2), we could observe an immediate neurite retraction (first 15 m), followed by a lag period and neurite regrowth. As a consequence, after 24 h of culture in these conditions, neurites of RTX-stimulated neurospheres were significantly shorter than untreated cultures ($p < 0.001$), vehicle control ($p < 0.01$) and RTX/CPZ-stimulated neurospheres ($p < 0.05$) (figures 3(d) and (f)). Notably, neurite length in vehicle control samples and RTX/CPZ-stimulated neurospheres was not significantly different ($p > 0.05$) than untreated cultures. Finally, we also measured cell metabolic activity after 24 h of culture under these conditions and observed that there was no significant difference ($p > 0.05$) among them, evidencing that despite neurite retraction, the neurons remain viable after RTX exposure (figure 3(g)). In sum, the differentiated nociceptors were electrically active and could sense and react to noxious stimuli.

3.3. Fabrication of 2D PN platform

3.3.1. 7 days culture

After characterization of nociceptor functionality, we developed a 3D biomimetic PN platform composed of a neurosphere/SCs co-culture on an aligned microfibrous scaffold (figure S6(a)). The scaffold is composed of aligned microfibers with an average diameter of 1.37 ± 0.20 μm and coherence (alignment degree) of 0.74 ± 0.04. To investigate the impact of the scaffold, we also cultured cells on glass coverslips and evaluated the performance of both substrates after 7 days of culture. The scaffold fibers generated aligned and elongated bands of SCs, in stark contrast to the flattened and isotropic morphology of SCs cultured on glass coverslips (figure S6(b)).

Neurospheres at day 9 of differentiation were placed on SC pre-cultured scaffolds/coverslips (one neurosphere per substrate) to establish the co-culture system. The effect of exogenous SCs on neurite growth and morphology was compared to coverslips/scaffolds that were uncoated, laminin-coated or matrigel-coated (figure 4). Uncoated coverslips did not even permit neurosphere attachment, while uncoated scaffolds allowed both neuron attachment and neurite outgrowth. This growth was however significantly shorter than all scaffolds with any form of coating ($p < 0.0001$) (figure S7(a)). When coverslips were pre-coated with laminin, matrigel or SCs, the neurospheres could attach and grow neurites (figure 4(a), left column). The neurosphere morphology depended on the coverslips coating, as the cluster remained intact when coated with laminin (figure 4(a) top left image) or seeded with SCs (figure 4(a) bottom left image), but not when coated with matrigel (figure 4(a) middle left image). In the latter, neurons dissociated from the cluster, proliferated and migrated outwards. As a result, we could not measure the axonal area, due to an unclear contrast between cell bodies and neurites. For the other two conditions, neurites were clearly emanating from the neurosphere and covered a total area of 3.6 ± 2.4% (laminin coating) or 3.4 ± 1.4% (SC seeding), not significantly different ($p > 0.05$) compared to uncoated scaffolds (2.4 ± 1.0%). When comparing neurite length, only coverslips with SCs were significantly higher compared to all other conditions ($p < 0.0001$) showing a mean length of 644.7 ± 258.2 μm (figure 4(B)). Regarding neurite alignment (figure 4(c)), coherence measurements indicated isotropic growth for all conditions with no significant differences between substrates.

By comparison, neurospheres cultured on scaffolds showed significantly increased ($p < 0.0001$) neurite length and overall neurite alignment compared to coverslips with equivalent coatings (figures 4(b) and (c)). Scaffolds coated with matrigel exhibited the longest neurite length (3071.0 ± 1568.0 μm) and highest coherence value (0.58 ± 0.09). SC-seeded scaffolds performed better than no coating or laminin-coated scaffolds, showing a mean neurite length of 1612.0 ± 491.0 μm compared to 544.3 ± 189.3 μm for no coating and 966.1 ± 378.2 μm for laminin and an alignment of 0.38 ± 0.06 in contrast with 0.20 ± 0.05 for no coating and 0.38 ± 0.12 for laminin; interestingly, scaffolds with no coating showed a statistically similar neurite length compared to growth on a SC-coated coverslip ($p > 0.05$), indicating that the lowest performing scaffold is equivalent to the optimal coverslip condition after 7 days of culture. Regarding axonal area, a matrigel coating led to a significantly larger scaffold coverage (13.3 ± 6.4%; $p < 0.001$) compared to laminin or SCs (3.4 ± 1.9% and 3.9 ± 2.4%, respectively), which was similar to coverslips. Scaffolds with no coating, resulted in a neurite area of 2.4%, the lowest value from all scaffold conditions.

SCs that were pre-seeded on either scaffolds or coverslips achieved an intimate association with neurites, although with clear differences regarding overall tissue organization (figure S6(c)). In coverslips (figure S6(c) top images), neurite projection was radial, isotropic and disorganized. Moreover, SCs tended to migrate towards the neurosphere, grouping around it in high density. In contrast, SCs seeded on scaffolds maintained their aligned morphology (figure S6(c) bottom images) and neurites appeared to follow the directional cues provided by the fiber topography and aligned SCs, leading to an organized and anisotropic pattern. In sum, scaffolds preserved the neuron clustering and promoted longer and more aligned neurite outgrowth compared to coverslips.

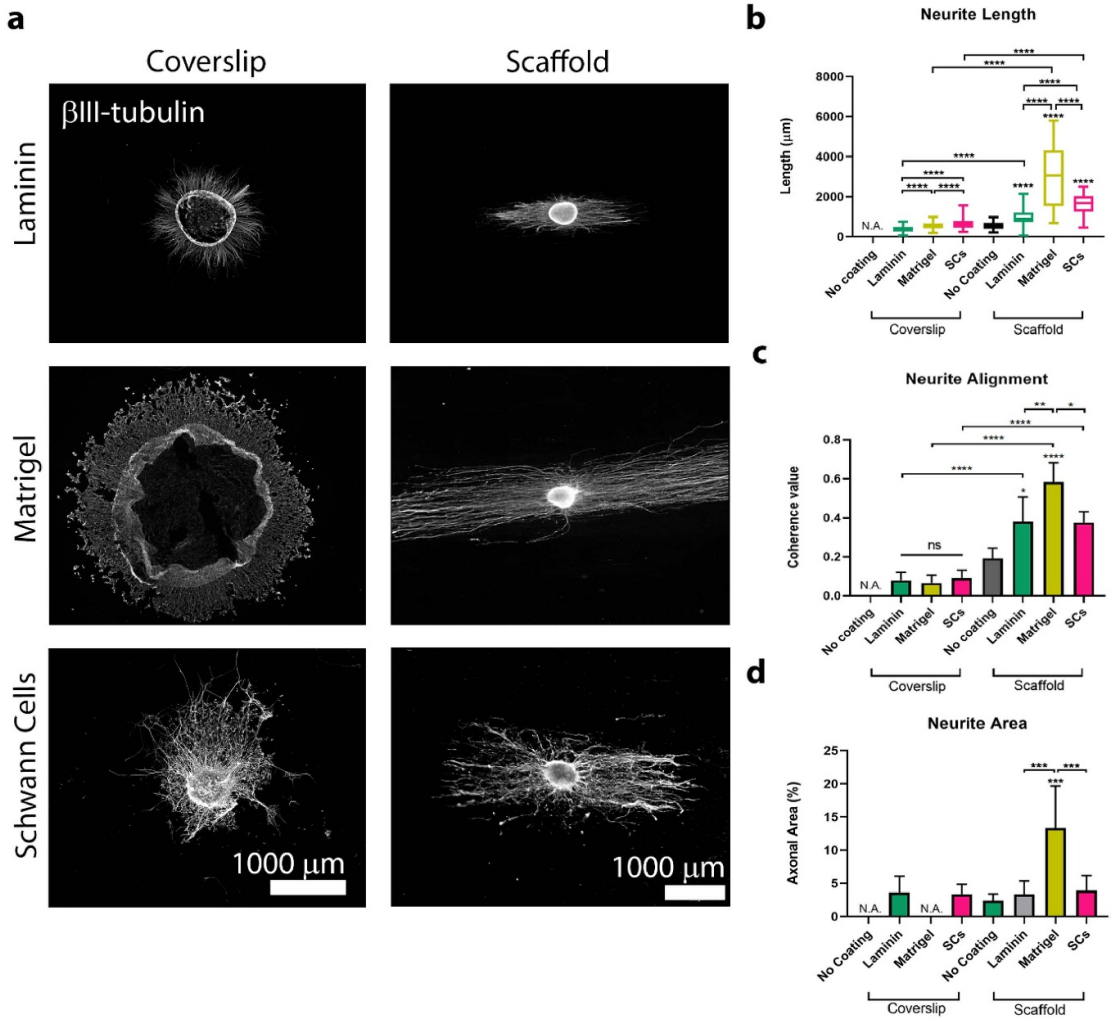

Figure 4. Characterization of neurosphere morphology in coverslips or scaffolds, with different coatings, after 7 days of culture. (A) Immunostaining to βIII-tubulin showing the overall axonal growth on coverslips (left column) or scaffolds (right column) coated with laminin (top row), matrigel (1:100 in DMEM; middle row) or SCs (bottom row). Quantification of (B) neurite length (in μm) (at least 15 measurements per sample), (C) neurite alignment (0 is full isotropy and 1 is full anisotropy) and (D) neurite area (% of total area). The boxplots represent data points between the minimum and maximum values. The graphs bars represent mean value $\pm$ SD. In all experiments, a minimum of five replicates were used per condition, and the experiments were performed twice. Statistics were performed with two-way ANOVA followed by a Tukey's HSD post-hoc test, where $^{****}p < 0.0001$, $^{***}p < 0.001$, $^{**}p < 0.01$, ns denotes $p > 0.05$. N.A. means not applicable. On the scaffold group, the stars with no associated bar represent comparisons with the no coating condition.

3.3.2. 21 days culture

After 21 days of culture, both neurite length and area increased compared to day 7. In coverslips cultures, SCs gradually led to neurosphere dissociation, similarly to the matrigel-coated coverslips, resulting in a neural network of multiple interconnected clusters; this hampered further axonal area quantification for both conditions. Only the laminin-coated coverslip preserved neurosphere integrity (figure 5(a) left column), with a neurite area of 12.4 $\pm$ 7.1% (figure 5(d)) and the longest neurite growth (mean length of 1335.8 $\pm$ 772.8 μm) of all coverslip conditions (figure 5(b)). From day 7 to day 21 (figure S8), we detected a 3.5-fold increase in growth for the laminin condition, whereas matrigel condition only imparted a 1.15-fold increase and the SCs condition registered a 0.69-fold decrease. This suggests that the maintenance of the neurosphere integrity is beneficial for enhanced neurite outgrowth, as cluster dissociation leads to the formation of a network with reduced outgrowth. Despite differences in growth, there was a generalized lack of preferred orientation with no differences in neurite alignment among conditions (figure 5(c)).

All scaffold cultures, including uncoated scaffolds, exhibited an increase in length and axonal area compared to the earlier time point (figure 5(a) right column, figures S7(b) and S8). In terms of neurite length this temporal increment corresponded to 1.61 times for uncoated, 2.2 times for laminin, 1.25 times for matrigel and 1.9 times for SCs samples (figure S8). Compared to coverslips cultures, the neurite length (figure 5(b)) was significantly enhanced ($p < 0.0001$) in all scaffold conditions. Matrigel-coated scaffolds promoted again the largest neurite extension, with a mean length of 3858.4 $\pm$ 1083.0 μm and area of

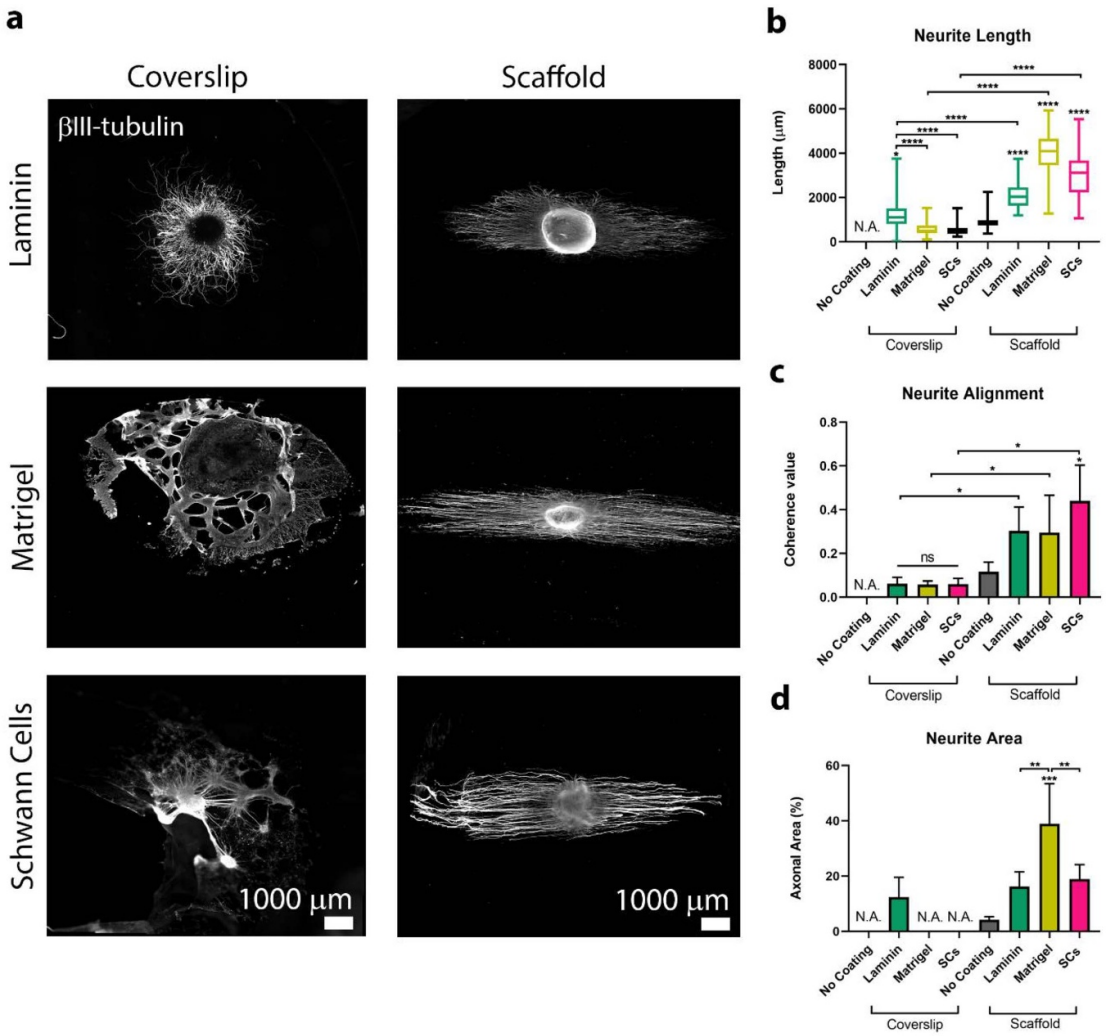

Figure 5. Characterization of neurosphere morphology in coverslips or scaffolds, with different coatings, after 21 days of culture. (A) Immunostaining to βIII-tubulin showing the overall axonal growth on coverslips (left column) or scaffolds (right column) coated with laminin (top row), matrigel (1:100 in DMEM; middle row) or SCs (bottom row). Quantification of (B) neurite length (in μm) (at least 15 measurements per sample), (C) neurite alignment (0 is full isotropy and 1 is full anisotropy) and (D) neurite area (% of total area). The boxplots represent data points between the minimum and maximum values. The graphs bars represent mean value $\pm$ SD. In all experiments, a minimum of five replicates were used per condition, and the experiments were performed twice. Statistics were performed with two-way ANOVA followed by a Tukey's HSD post-hoc test, where $^{****}p < 0.0001$, $^{***}p < 0.001$, $^{**}p < 0.01$, ns denotes $p > 0.05$. N.A. means not applicable. On the scaffold group, the stars with no associated bar represent comparisons with the no coating condition.

38.9 $\pm$ 14.6%, followed by SC-seeded scaffolds with a mean length of 3076.5 $\pm$ 995.8 μm and area of 18.95 $\pm$ 5.2%, then laminin-coated scaffolds with a mean length of 2130.1 $\pm$ 619.4 μm and area of 16.21 $\pm$ 5.3% and finally uncoated scaffolds with a mean length of 878.1 $\pm$ 292.3 μm and area of 4.16 $\pm$ 1.16% (figures 4(b) and (c)).

In the early stages (up to 7 days), SCs promote a more accelerated neurite outgrowth compared to laminin coatings, but this growth tends to slow down as SCs begin to myelinate axons. Since myelination results in thicker and straighter segments [30] (figures 6(a) and S9), this hypothetically explains why we detected the highest neurite alignment for SC-seeded scaffolds (0.44 $\pm$ 0.16) (figure 5(a)). All scaffold conditions at 21 days *in vitro* (DIV) led to increased ($p < 0.05$) alignment compared to similarly coated coverslips.

For both coverslips and scaffolds, myelination was observed by day 21 as an abundance of MBP$^+$ segments that spatially correlated with βIII-tubulin$^+$ structures (figure 6). Unmyelinated cultures, i.e. cultures devoid of SCs, did not have MBP$^+$ segments (figure S10). In coverslips, the myelin was disorganized, randomly oriented and partially overlapping (figures 6(a), S9(a) and (b)). These myelinated cultures were mechanical unstable, attributed to the high lipid content that results in poor surface attachment (data not shown). On the other hand, co-cultures in scaffolds resulted in long, straight and anisotropic myelin bundles (figure 6(a) bottom image), with overall great mechanical stability. The presence of

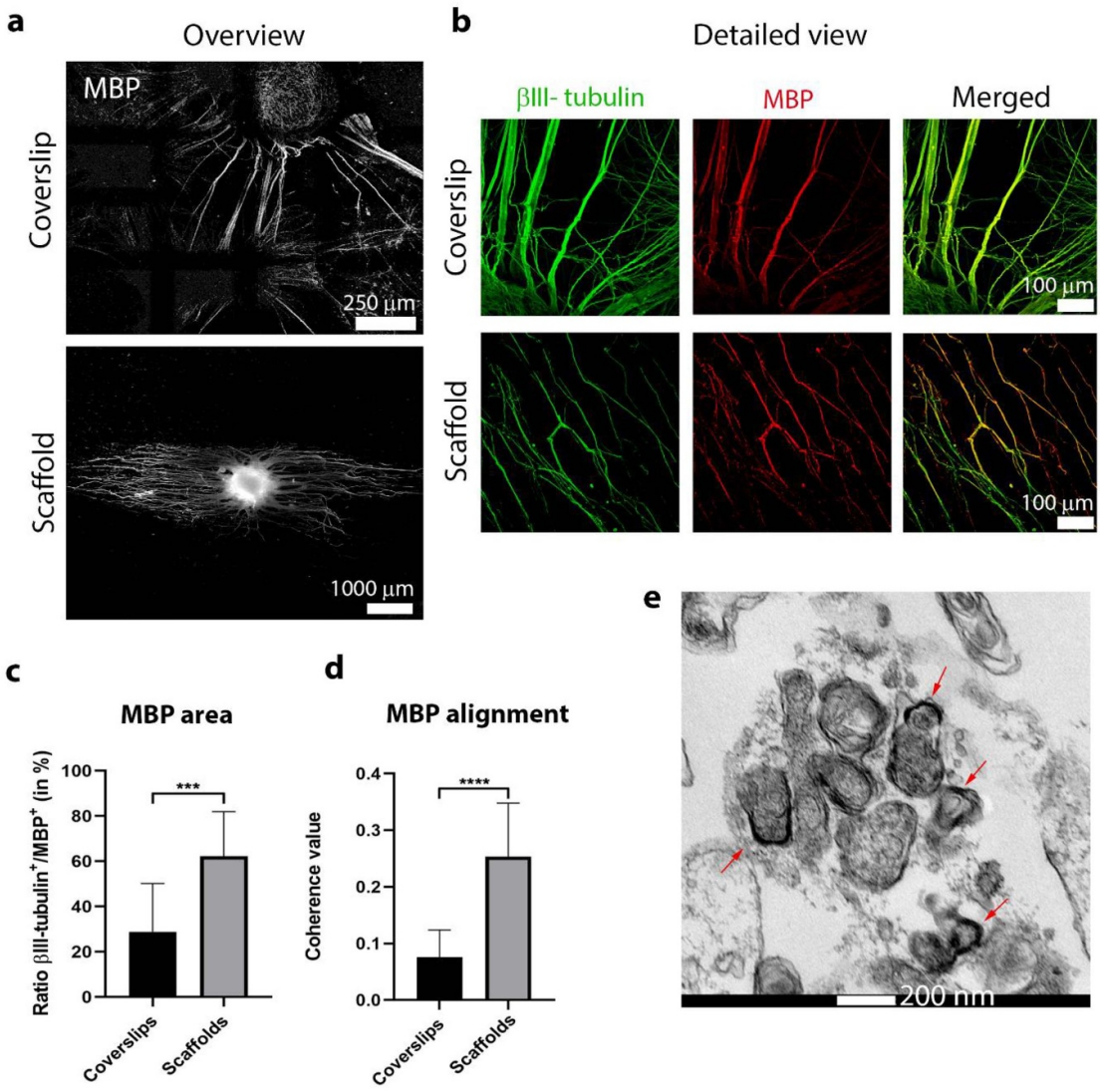

Figure 6. Myelin visualization and quantification of neurosphere/SCs co-cultures on coverslips or scaffolds for 21 days. (A) Overview of myelin segments (marked by myelin basic protein (MBP) in gray) on coverslips (top) and scaffolds (bottom). The shadow lines visible in the top image are imaging artifacts resultant from tile merging. (B) Detailed view of myelin segments from coverslips (top row) or scaffold cultures (bottom row), showing the co-localization of neurites (left column; βIII-tubulin staining in green) and myelin (middle column; MBP in red). (C) MBP area (% of βIII-tubulin^{+} area /MBP^{+} area). (D) MBP alignment (0 is full isotropy and 1 is full anisotropy). Both graph bars show the mean value $\pm$ SD. (E) TEM micrograph of a myelin cross section, from a 21 days old scaffold co-culture, depicting compact and thick myelin layers (average thickness is 89.1 $\pm$ 17.6 nm). The red arrows point to spots where the presence of compact myelin is visible. Scale bar is 200 nm. These experiments were performed twice ($n = 5$). For imaging analysis, we took at least five images per sample. Statistics were performed with an unpaired t-test, where $^{****}p < 0.0001$ and $^{***}p < 0.001$.

other mature myelin proteins, such as myelin protein zero (P0) was also detected (figure S8(c)).

Quantification of myelin formation and morphology revealed that scaffolds had a larger myelin area (62.2 $\pm$ 19.73% versus 28.78 $\pm$ 21.34% in coverslips; figure 6(c)) and improved myelin alignment (0.25 $\pm$ 0.09 versus 0.07 $\pm$ 0.05 in coverslips; figure 6(d)). Further in-depth TEM analysis of a scaffold cross-section (figure 6(e)) detected the presence of several compacted myelin layers, with an average thickness of 89.1 $\pm$ 17.6 nm.

In brief, scaffolds promoted a continuous neural growth and long-term stability of the cluster, as well as longer and more aligned neurites than coverslips. Myelination was also enhanced and more anisotropic in scaffold co-cultures.

3.4. Hyperglycemia model and drug testing

After establishing the myelinated co-culture scaffold platform, we investigated hyperglycemia-induced damage on myelin and evaluated the mitigating effect of epalrestat, an aldose reductase inhibitor [31] (figure 7(a)). After 21 days of co-culture, the cells were cultured for 48 h in just hyperglycemia (45 mM glucose) or hyperglycemia plus epalrestat (glucose at 45 mM plus epalrestat at 1 μM); normal neural medium was used as control. As shown in figure 7(b), control cultures (left column) and

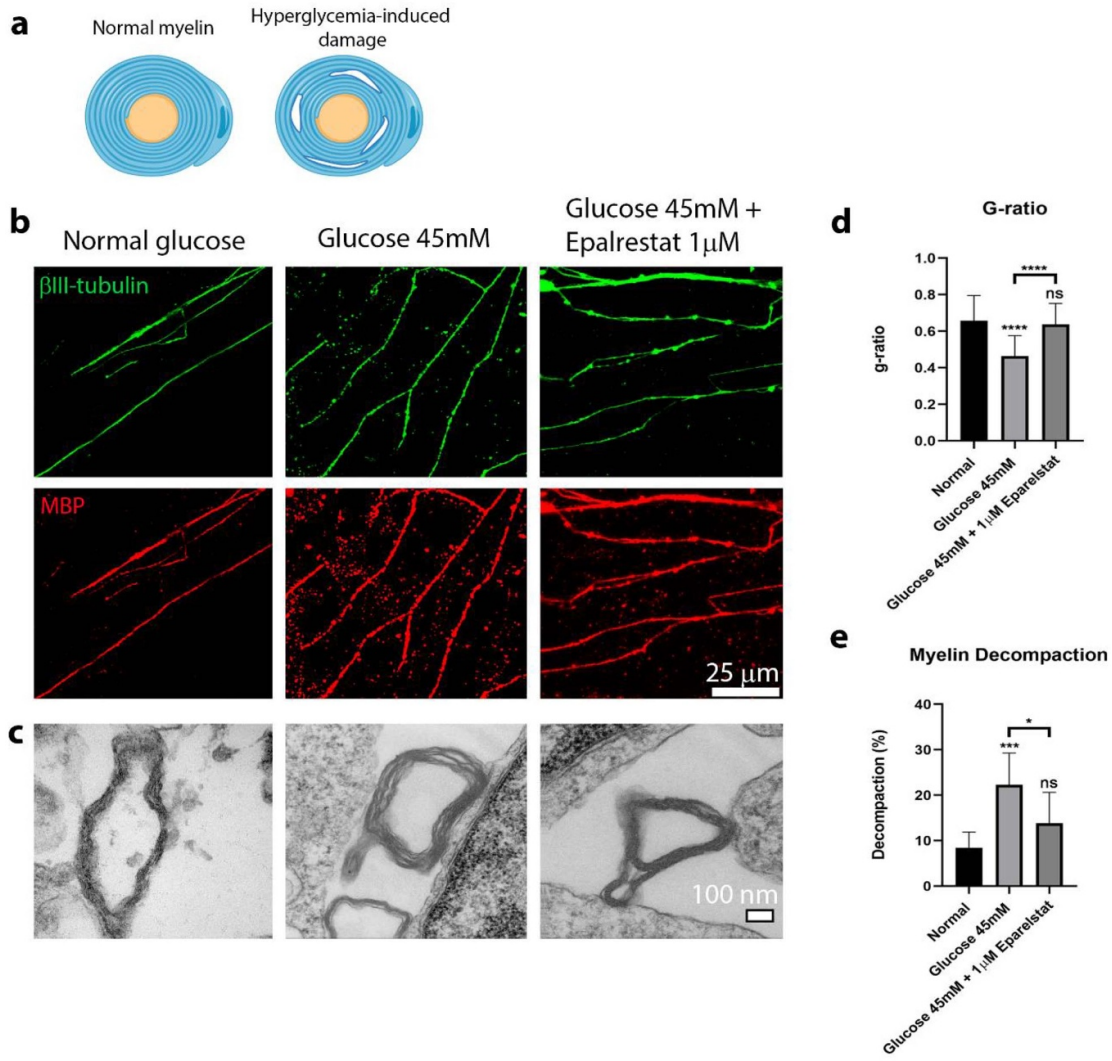

Figure 7. Hyperglycemia-induced damage and epalrestat prevention, on 21 days scaffold co-cultures. (A) Illustration of the myelin morphology in normal (left image) or hyperglycemic (right image) state, where aberrations such as layer decompaction are present. At day 21, co-cultures were treated for 48 h with glucose (45 mM) (middle column) or glucose (45 mM) + epalrestat (1 μM) (right column) within neural medium. Untreated cells (normal medium) were used as control. (B) Immunostaining for βIII-tubulin (green, top row) and MBP (red, bottom row) shows that exposure of myelinated cultures to high glucose concentrations leads to myelin damage. However, when epalrestat is supplemented, myelin disruption can be mitigated. (C) TEM micrographs of myelin cross sections, evidencing myelin layers decompaction and abnormalities in hyperglycemic conditions. In normal conditions or hyperglycemic conditions containing epalrestat, myelin appears normal. (D) *G*-ratio and (E) myelin decompaction measurements from TEM micrographs, shown as mean value $\pm$ SD. Experiments were performed twice ($n = 4$). Statistics were obtained with one-way ANOVA followed by a Tukey's HSD post-hoc test, where $^{****}p < 0.0001$, $^{***}p < 0.001$, $^{*}p < 0.05$ and ns means $p > 0.05$.

those supplemented with epalrestat (right column) appeared normal, with no significant damage. Contrarily, hyperglycemia cultures (middle column) showed signs of myelin disruption, particularly visible by MBP immunostaining (in red). TEM micrographs of control cultures (figure 7(c) left image) revealed compact myelin layers with no particular irregularities. In hyperglycemia cultures (figure 7(c) middle image), it was particularly evident that myelin layers separated from each other, exhibiting a decompacted structure. Finally, myelin morphology in hyperglycemia with added epalrestat condition (figure 7(c) right image) resembled control cultures, with most layers well compacted and with no signs of abnormalities. TEM images were quantified according to *g*-ratio, a standard parameter, and myelin decompaction percentage, based on an established algorithm [20]. *G*-ratio measurements showed that both control and glucose plus epalrestat groups produced similar results, with a *g*-ratio value of 0.66 and 0.63, respectively (figure 7(d)). The glucose-only group produced a lower value of 0.46 ($p < 0.0001$), due to myelin layer decompaction. This was reflected in the myelin decompaction measurements, where the control group had the lowest decompaction (8.4%), the hyperglycemic condition had the highest decompaction (22.2%), and the condition of hyperglycemia with epalrestat registered decompaction

value (13.8%) that was equivalent to control and significantly lower than hyperglycemia alone ($p < 0.05$).

In sum, hyperglycemia induce myelin damage, evidenced by layer decompaction, which could be mitigated with epalrestat supplementation.

3.5. Development of a large PN biomimetic platform

To develop a more representative model that better emulates the 3D hierarchical microarchitecture of a PN, scaffolds containing neural and glial tissue were embedded in a fibrin hydrogel. In the 3D image reconstructions shown in figure 8(a), scaffolds with no hydrogel generated an anisotropic and planar neurite growth (figure 8(a) left column) with only a small volume increase from day 7 to day 21, from 0.0025 to 0.0039 μm^3, respectively (figure 8(b)). When co-cultures were supplemented with fibrin, neurite growth maintained directional alignment (similar to all conditions and time points, figure S11) but was notably multiplanar (figure 8(a) right column), with still a small increase overtime but comparatively larger than bare scaffolds at both 7 DIV (~3 fold; 0.0078 μm^3) and 21 DIV (~2 fold; 0.0094 μm^3) (figure 8b and movie S4). Fibrin embedding also promoted a significant increase ($p < 0.001$) of myelin volume at day 21 compared to scaffold-only co-cultures (figure 8(c)), with a mean myelin volume of 0.0012 μm^3 versus 0.00046 μm^3, respectively. This was also reflected in histological cross-sections (figure 8(d)), which showed a larger number of myelin rings in fibrin-scaffolds than in bare scaffolds.

To showcase the long-term development and stability of this fibrin-embedded platform, we maintained the co-cultures for 35 days and evaluated the resulting tissue morphology. The engineered neural tissue retained its 3D organization and exhibited highly aligned myelinated axons that achieved over 6.5 mm in length in all growth planes (figures 8(e) and (f)), which is the largest reported value in literature, to the best of our knowledge.

3.6. Applicability for target tissue innervation

To demonstrate the potential use of the fibrin PN platform for the creation of innervated tissue models, we show here the possibility of adding pancreatic pseudoislets (figures 9(a)–(d)) and endometrial organoids (figures 9(e)–(h)) within the construct. Pancreatic pseudoislets were generated with a mean diameter of 41.9 ± 2.98 μm (figures S12(a) and (b)), composed of alpha (alpha TC1) and beta cells (INS1E) at a ratio of 3:7 [32]. Neurospheres were cultured on laminin-coated scaffolds for 7 days to initiate neural growth, after which several pancreatic pseudoislets were added and the entire construct embedded in fibrin. The co-cultures were maintained for an additional 10 days, during which time the pseudoislets survived and nociceptors from the neurospheres extended and surrounded them (figures 9(c) and (d)). Further reflecting native rodent pancreatic tissue, alpha (glucagon$^+$; in green) and beta cells (insulin$^+$; in red) reorganized and formed segregated clusters according to cell type [33]. Immunostaining for substance P (white) revealed that nociceptor axons were able to penetrate the cluster and establish an intimate association with the pancreatic cells, particularly insulin$^+$ cells.

To create an endometrium model, a GFP$^+$ human endometrial adenocarcinoma cell line (Ishi-M3-HSD-A) [23] was seeded within matrigel domes to form organoids of regular size, with a mean diameter of 59.9 ± 12.1 μm (figures 9(e)–(f), S12(c) and (d)). Matrigel domes containing several organoids were picked and positioned on a laminin-coated scaffold in the vicinity of a 7 DIV neurosphere. After 10 days, we confirmed that the endometrial organoids attached, survived, and retained their spherical shape throughout the co-culture period (figure S13). Nociceptor neurites were able to penetrate through the matrigel domes and establish an intimate association with endometrial cells (figures 9(g), (h), and S13).

3.7. Discussion

Nociceptive pain perception is essential for normal organ function and physical integrity maintenance. However, sensory nerves can be affected by a multitude of insults, ranging from trauma to disease-induced neuropathies, which hinder this sensorial ability. At the same time, nociceptive pain is a common symptom of a large range of pathologies, bringing discomfort and reduced life quality to diseased individuals. Current understanding of neuropathies and pain mechanisms in a pathological context is limited by current research tools, which consist of animal models or oversimplified 2D *in vitro* models. Animal models are expensive, difficult to assess and are not always clinically translatable to humans [34]. *In vitro* models, on the other hand, can provide an inexpensive, simple and direct translational research platform [35]. To date, some *in vitro* human nociceptor models, containing neurons that are able to elicit APs and are sensitive to noxious stimuli, have already been reported [13, 14]. However, the tissue in these models does not replicate the 3D anisotropic axonal morphology that characterizes the PN. Moreover, the reported neurons are unmyelinated, which represents only the slow transmission nociceptors (C-fibers) and not the myelinated fast transmission fibers (Aδ) [1, 2]. This lack of proper architectural and cellular representation limits the translational potential of the models and demands for improved biomimetic PN platforms.

In this work, we demonstrate the fabrication of a 3D culture platform containing functional iPSCs-derived nociceptors neurospheres with myelinated or unmyelinated anisotropic neurites. To

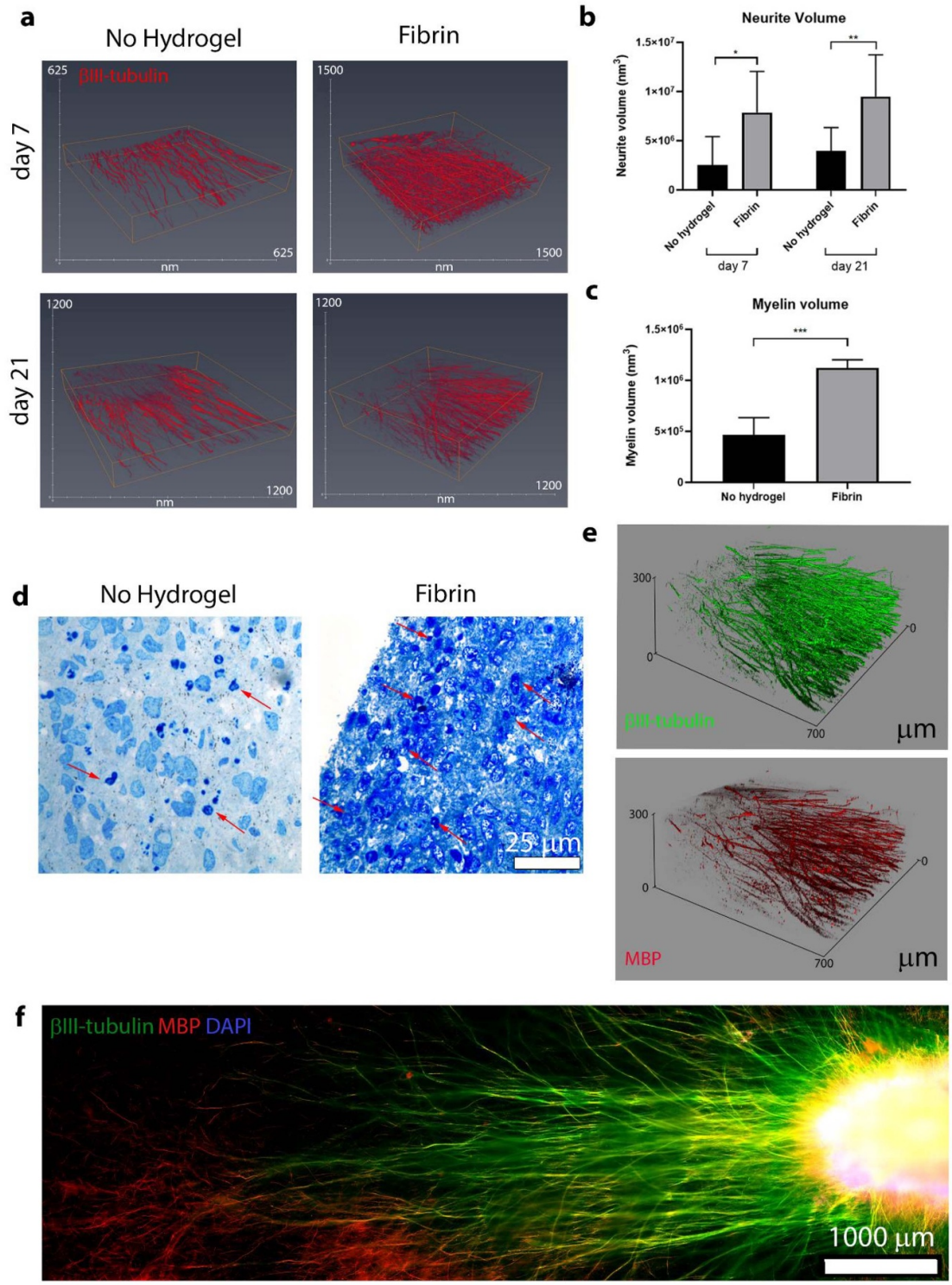

Figure 8. Enhancement of the PN platform via fibrin hydrogel addition on the neurosphere/SC scaffold co-culture. (A) 3D reconstruction of the neurite volume of neurospheres embedded with (right column) or without (left column) fibrin at 7 days (top row) and 21 days (bottom row) of culture. (B) Quantification of the neurite volume in cultures with (gray bars) and without (black bars) fibrin embedding at 7 (left side) and 21 (right side) days of culture, indicating that fibrin addition significantly increased neurite volume. (C) Quantification of the myelin volume in cultures with (gray bars) and without (black bars) fibrin embedding at 21 days of culture, showing an increase in myelin volume in cultures embedded with fibrin hydrogel. In both (B) and (C), the graph bars are represented as mean value ± SD. Experiments were performed twice ($n = 5$). Statistics were performed with two-way ANOVA followed by a Tukey's HSD post-hoc test (B) or an unpaired t-test (C), where $^{***}p < 0.001$, $^{**}p < 0.01$ and $^{*}p < 0.05$. (D) Toluidine blue–stained tissue sections showing myelin cross-sections in dark blue (pointed by red arrows), evidencing a higher density of dark blue spots in the fibrin condition. Scale bar is 25 μm. (E) 3D reconstruction of a neurosphere/SCs platform cultured with fibrin for 35 days, showing the formation of layered and highly aligned myelinated neurites. (F) Overview of the growth of a 35 DIV co-culture, showing the formation of highly aligned and long (over 6.5 mm) neurites throughout the platform. For (E) and (F) βIII-tubulin is shown in green, MBP in red and DAPI in blue.

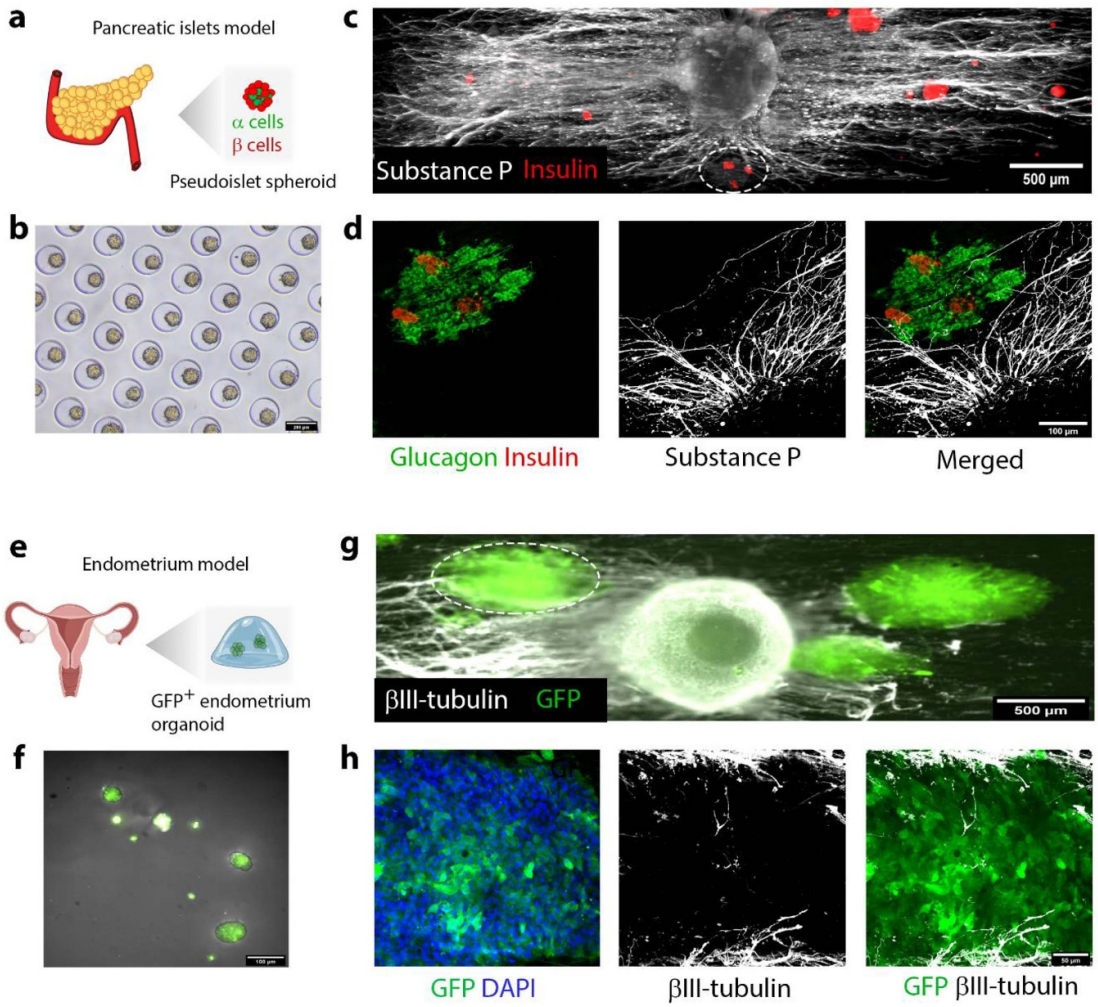

Figure 9. Nociceptor innervation of target tissues within the fibrin-embedded PN platform. (A)–(D) Pancreatic pseudoislets innervation. (A) Illustration of the used pancreatic islet model composed of α cells (alpha TC cells) and β cells (INS1E cells) at 3:7 ratio respectively. (B) Agarose microwell mold containing several spheroids with 41.9 ± 2.98 μm. Scale bar is 200 μm. (C) Overview of the platform showing the presence of several pancreatic pseudoislets (insulin, red) surrounding the neurosphere (substance P, white). (D) Detailed view of the white dashed ellipse shown in (C) showing infiltrating nociceptor fibers within the pseudoislets. Glucagon is shown in red and DAPI in blue. Scale bar is 500 μm for (C) and 100 μm for (D). (E)–(H) Endometrial organoid innervation. (E) Illustration of the endometrial model composed of GFP^+ Ishikawa organoids formed within matrigel domes. (F) Brightfield image superimposed with the green fluorescent channel showing the cultured endometrium organoids, with a diameter of 59.9 ± 12.1 μm. Scale bar is 100 μm. (G) Overview of the co-culture platform showing several organoids (GFP, green) around the neurosphere (βIII-tubulin). (H) Detailed view of the white dashed ellipse shown in (G), depicting neurite invasion on the endometrial organoid. DAPI is shown in blue. Scale bar is 500 μm in (G) and 50 μm in (H).

produce these neurospheres we modified the protocol described by Chambers *et al* for accelerated conversion of iPSCs into nociceptors [19]. In our two-step method, we started by seeding iPSCs on an agarose microwell device that induces the formation of spheroids via cell self-aggregation. Because of this, we were able to generate a large number of uniformly sized cell clusters (over 1500) that form a miniature version of a DRG [36]. With an average size of $\sim$300 μm, the neuron cluster is sufficiently large to generate dense and long neuronal tissue, but still sufficiently small to rely on diffusion alone for oxygen and nutrient support. Additionally, at this size, the neurospheres are easily observable with a naked eye, and thus can be picked and transplanted into a desired location on the scaffold (figure 1 and 2D). Contrarily, other nociceptor differentiation protocols culture cells on flat surfaces, producing disorganized and non-homogeneous cultures [19, 37]. Before commencing differentiation, we adopted a strategy for cell synchronization via DMSO treatment, which has been reported as an effective method to arrest the iPSCs cycle and simultaneously maintain their pluripotency characteristics [38]. Following this, the differentiation protocol was initiated and after 7 days cells exhibited a trunk NC phenotype (figures 2(b) and (c)). Contrary to Chambers *et al* protocol, we supplied retinoic acid after day 2, which has been reported as a promoter of trunk NC specification [27] and enhanced the spheroids cohesion (figure S2(b)). At day 9 of differentiation, the neurospheres were harvested for the second part of the process, where these

were placed on the desired culture substrate and cultured for at least 7 days, to simultaneously promote maturation to a nociceptor phenotype and neurite outgrowth on the substrate. The use of neurotrophic factors in this last stage was reduced to just NGF, which proved enough to promote growth and phenotype acquisition. In just a 3 week period, we were able to obtain several neurospheres (over 1500) exhibiting characteristic nociceptor markers such as substance P, CGRP and TRPV-1 expression (figure 2(e)). The obtained neurons were electrically active, presenting an RMP value slightly higher than other reported iPSCs neurons [39, 40], but all able to elicit APs when stimulated (40 DIV cultures; figure 3(a) and table S2). These differentiated nociceptors also released substance P in response to a noxious stimulus (RTX) (10 DIV cultures; figure 3(b)), denoting the presence of a functional TRPV-1 channel [28, 37]. For these experiments, we used dissociated neuron cultures in order to improve the access of the electrical probe to single cells and ensure that substance P release was unhindered by the cell cluster. Clustered nociceptors, representing a more biomimetic form, also revealed functionality, as shown by the reversible RTX-induced neurite retraction from 7 DIV neurospheres (movie S2). RTX (or capsaicin) activation of TRPV-1 promotes calcium influx, which in turn can lead to mitochondrial dysfunction and inhibition of metabolism, resulting in the collapse of nerve endings [41]. This effect is observed on the skin, where after topical capsaicin treatment, epidermal nociceptor fibers are reversibly lost [29]. We could replicate this process using RTX, and additionally, neurite retraction could be significantly reduced by co-addition of a TRPV-1 antagonist (CPZ) (figures 3(d)–(f) and movie S3). After 24 h, all conditions showed similar metabolic activity (figure 3(g)), evidencing that nociceptors neurites can be targeted, without loss of viability, using an RTX sub-toxic application (10 μM).

After establishing nociceptor functionality, we developed a PN model that replicates the native morphology using an aligned microfibrous scaffold (figure 1), which we previously reported as suitable to induce anisotropic neurite and myelin formation from rat DRGs and PC12 cells [20]. Unlike other strategies that rely on platform wall constraining to induce axonal alignment [16, 17], we simply used a substrate whose fibers are highly efficient in directing parallel axonal growth. Moreover, the fibers coating can be easily customized, which endows the platform with high versatility regarding the chemical and cellular composition. To recreate a PN tissue, we pre-seeded the scaffold with SCs, which proliferated and organized in highly aligned cell bands within 7 days (figure S6(b)). These SC bands replicate the native bands of Büngner, which form in the regenerating PN, to stimulate and guide regrowing axons to their targets [42]. As a cell source, we used the rat sciatic nerves, from which SCs can be extracted in high yield, are easily purified [21], and have been shown to efficiently myelinate human iPSC-derived sensory neurons [15]. To better evaluate the influence of SCs in promoting neural growth, we compared them with scaffolds coated with laminin (major nerve extracellular matrix (ECM) protein) [43] and matrigel (assortment of ECM proteins) [44], which are standard coatings in *in vitro* PN models [5]. Matrigel-coated scaffolds promoted the highest neural growth followed by SCs-containing scaffolds, which additionally were composed of vast and anisotropic myelinated neurites. Compared to glass coverslips, our scaffolds promoted higher neurite length, alignment and area after 7 and 21 days of culture (figures 4 and 5). Scaffolds also displayed larger amounts of myelin and more aligned segments than coverslips cultures (figure 6), and in both substrates we observed myelination of small caliber axons (<1.5 μm) similarly to other reported works [15, 45]. Furthermore, in all scaffold coatings the neuron cluster remained intact, which allowed a neurite outgrowth comparable to a DRG explant. Contrary to this, matrigel coated coverslips promoted neurosphere dissociation already at 7 DIV, and SC-seeded coverslips showed a similar morphology after 21 DIV. Because matrigel is composed of an abundant mixture of ECM molecules and growth factors, which have been shown to be involved in neuronal proliferation/migration, as is the case of entactin and transforming growth factor beta (TGF-β) [46, 47], we hypothesize that its coating on coverslips led to the observed cluster break and neuron spread. In the case of SC-seeded coverslips, we believe that the unconstrained SC proliferation and migration (figure S6(C)), and subsequent ECM deposition, led to a similar neuron morphology overtime. On the other hand, the scaffold's aligned microfibers facilitated cell entrapment, prevented cluster dissociation, and induced anisotropic neural growth [48–50].

Uncoated substrates, i.e. not containing any adhesive units, such as laminin, are traditionally not supportive of neuron attachment, survival and growth [51]. However, uncoated scaffolds supported neural growth (figure S6) while uncoated coverslips could not even allow cell attachment. This can be explained by the abovementioned scaffold's topographical properties but also its chemical composition, since polyethylene oxide taraphtalate (PEOT/PBT) does not require functionalization to allow nerve growth [52], contrary to glass [51]. In sum, our scaffold provided a superior substrate than glass coverslips, by promoting PN tissue development with higher efficiency, robustness and biomimicry level.

Using the scaffold co-culture system, we produced myelinated tissue to investigate the resulting damage from acute hyperglycemia exposure. Hyperglycemia is a common pathophysiological imbalance resulting

from diabetes mellitus type II and a cause of peripheral neuropathy [7, 53]. In this situation, excess intracellular glucose is converted to sorbitol by aldose reductase, resulting in sorbitol accumulation, and consequently in increased cellular osmolarity, oxidative stress and mitochondrial dysfunction that leads to cellular damage [8, 53, 54]. Hyperglycemia damage is characterized by axonal degeneration and myelin abnormalities, such as layer decompaction [54, 55] (figure 7(a)). Thus, morphological evaluation can be used to determine the presence of damage, and if so, if it can be prevented by drug supplementation. Among the existing drugs, aldose reductase inhibitors such as epalrestat, have been explored as a method to reduce sorbitol levels, with shown influence in mitigating hyperglycemic damage [8, 31]. To achieve an acute hyperglycemic state, supraphysiological glucose concentrations (45 mM) can be supplied in the culture medium, allowing a rapid modeling of blood glucose spikes [20]. In our experiment, acute hyperglycemic exposure caused axonal and myelin damage, morphologically similar to diabetic type II mice [8], which was quantitatively manifested in increased layer decompaction and decreased *g*-ratio (due to layer separation), compared to control cultures. Supplementation of epalrestat to hyperglycemic cultures effectively mitigated the cellular damage, denoting a benefit of sorbitol reduction in damage prevention (figure 7). These results highlight the advantages that *in vitro* platforms provide in comparison to animal models, by permitting a rapid, simple and inexpensive but still accurate modeling of pathologies, as well as testing of therapeutic compounds. Additionally, in diabetic animal models there are several physiological processes altered at once, causing a systemic damage that reduces the level of experimental control and undermines data reliability [55, 56]. Although we observe myelination of small caliber axons in our *in vitro* 3D platform, myelination of axons smaller than 1.5 μm remains a controversial finding and should be investigated further in-depth and corroborated in future studies. This will be greatly assisted by advances in analytical techniques, such as the use of third harmonic imaging (THI) to directly visualize the 3D structure of axon myelination of living cells [57]. While still rarely applied, such label-free approaches avoid preparation artifacts associated with more established techniques, such as TEM, and provide more accurate 3D analysis of myelin wrapping for thicker tissue constructs compared to wide-field or confocal fluorescence microscopy.

To develop a more biomimetic PN model, we embedded the cell-seeded scaffold in a fibrin hydrogel. Fibrin is a natural material present during nerve regeneration and widely used within PN conduits and models [58, 59]. Its addition permitted neurites to grow beyond the scaffold, resulting in a neurite and myelin volume enhancement compared to bare scaffolds, while maintaining anisotropy (figure 8 and movie S4). The formation and maintenance of an overall neural tissue alignment suggests that the topographical guidance provided by the scaffold fibers and SCs at the bottom of the substrate is sufficient to direct anisotropy throughout the whole construct. As hypothesized in a previous work from our group [20], we believe that a combination of attractive and repulsive paracrine cues are governing this phenomenon, by propagating the neurite alignment from the bottom to the upper layers. This suggests that the topographical guidance provided by the scaffold, at the bottom of the construct, is sufficient to induce an overall neurite alignment, in a process potentially governed by axonal paracrine signaling [20, 60, 61]. Using the fibrin/scaffold PN platform, we demonstrated the ability to create myelinated tissue with long-term stability and exhibiting neurite dimensions (over 6.5 mm), which are to the best of our knowledge, the highest ever reported in *in vitro* platforms [16, 62].

Finally, as a proof-of-concept, we demonstrated that different target tissues can be incorporated within the fibrin/scaffold PN platform, with the aim of generating nociceptor innervation models. As targets, we selected the pancreas, represented by pancreatic pseudoislets, and the endometrium, represented by endometrial organoids. Both the pancreas, during CP [9, 10], and the endometrium, during endometriosis [63, 64], are innervated by unmyelinated nociceptors, which can become sensitized and trigger nociceptive pain. However, the exact pain pathophysiological mechanisms remain to be elucidated and current research is exclusively conducted in animal models, due to a lack of representative *in vitro* models. In this work, we established culture conditions that permitted simultaneous survival of all tissues and nociceptor ingrowth towards the target tissue, within 10 days of co-culture (figure 9). We did not further explore the mechanisms of nociceptor innervation or sensitization, as we merely intended to show the potential and versatility of this platform in generating various nociceptor innervation models. Future studies should aim at decoding the biological processes governing neural target/tissue interactions, such as tissue-specific pain mechanisms, as well as screening of compounds with therapeutical/analgesic properties. Using this platform, such studies could be conducted in a safe, convenient, quick and inexpensive manner.

In summary, we demonstrate here the formation of a 3D biomimetic nociceptor platform that can be used to assess neural growth in fine-tuned microenvironments, to model diabetes-related pathologies and to produce innervation models. We believe that this platform could provide a new highly relevant tool for neuroscience and for biomedical sciences in general.

Data availability statement

The authors declare that all data supporting the findings of this study are available within the paper and in Supplementary Information, and are also available from the corresponding author upon reasonable request.

Acknowledgments

We thank the Microscopy CORE Lab (M4I Maastricht University), especially Hans Duimel and Kevin Knoops for their help in TEM and confocal imaging. We also thank the province of Limburg for the project funding. This work was partly supported by the research programme VENI 2017 STW- project 15900 financed by the Dutch Research Council (NWO).

ORCID iDs

Adrián Seijas-Gamardo https://orcid.org/0000-0002-8950-367X
Paul Wieringa https://orcid.org/0000-0002-3290-5125
Lorenzo Moroni https://orcid.org/0000-0003-1298-6025

References

[1] Inquimbert P and Scholz J 2012 *Pain. Basic Neurochemistry* (Amsterdam: Elsevier) (https://doi.org/10.1016/b978-0-12-374947-5.00067-5)
[2] Dubin A E and Patapoutian A 2010 Nociceptors: the sensors of the pain pathway *J. Clin. Invest.* **120** 3760–72
[3] Zieglgänsberger W 2019 Substance P and pain chronicity *Cell Tissue Res.* **375** 227–41
[4] Frias B and Merighi A 2016 Capsaicin, nociception and pain *Molecules* **21** 797
[5] Wieringa P A, Gonçalves de Pinho A R, Micera S, van Wezel R J A and Moroni L 2018 Biomimetic architectures for peripheral nerve repair: a review of biofabrication strategies *Adv. Healthcare Mater.* **1701164** 1–19
[6] Rajchgot T, Li R-H, Ma L, Li N, Shan P-Y, Wang X-B and Liu A-F 2019 Neurons and microglia; a sickly-sweet duo in diabetic pain neuropathy *Front. Neurosci.* **13** 1–17
[7] Yagihashi S, Mizukami H and Sugimoto K 2011 Mechanism of diabetic neuropathy: where are we now and where to go? *J. Diabetes Invest.* **2** 18–32
[8] Hao W *et al* 2015 Hyperglycemia promotes Schwann cell de-differentiation and de-myelination via sorbitol accumulation and Igf1 protein down-regulation *J. Biol. Chem.* **290** 17106–15
[9] Li Q and Peng J 2014 Sensory nerves and pancreatitis *Gland Surg.* **3** 284–92
[10] Atsawarungruangkit A 2015 Current understanding of the neuropathophysiology of pain in chronic pancreatitis *World J. Gastrointest. Pathophysiol.* **6** 193
[11] Demir I E, Tieftrunk E, Maak M, Friess H and Ceyhan G O 2011 Pain mechanisms in chronic pancreatitis: of a master and his fire *Langenbeck's Arch. Surg.* **396** 151–60
[12] Zondervan K T, Becker C M, Koga K, Missmer S A, Taylor R N and Viganò P 2018 Endometriosis *Nat. Rev. Dis. Primers* **4** 1–25
[13] Wainger B J *et al* 2015 Modeling pain *in vitro* using nociceptor neurons reprogrammed from fibroblasts *Nat. Neurosci.* **18** 17–24
[14] Jones I, Yelhekar T D, Wiberg R, Kingham P J, Johansson S, Wiberg M and Carlsson L 2018 Development and validation of an *in vitro* model system to study peripheral sensory neuron development and injury *Sci. Rep.* **8** 1–15
[15] Clark A J, Kaller M S, Galino J, Willison H J, Rinaldi S and Bennett D L H 2017 Co-cultures with stem cell-derived human sensory neurons reveal regulators of peripheral myelination *Brain* **140** 898–913
[16] Sharma A D, Da Rocha G O and de Andrade J B 2019 Engineering a 3D functional human peripheral nerve *in vitro* using the nerve-on-a-chip platform *Sci. Rep.* **9** 1–12
[17] Uzel S G M, Platt R J, Subramanian V, Pearl T M, Rowlands C J, Chan V, Boyer L A, So P T C and Kamm R D 2016 Microfluidic device for the formation of optically excitable, three-dimensional, compartmentalized motor units *Sci. Adv.* **2** 1–13
[18] Osaki T, Uzel S G M and Kamm R D 2018 Microphysiological 3D model of amyotrophic lateral sclerosis (ALS) from human iPS-derived muscle cells and optogenetic motor neurons *Sci. Adv.* **4** 1–16
[19] Chambers S M *et al* 2012 Combined small-molecule inhibition accelerates developmental timing and converts human pluripotent stem cells into nociceptors *Nat. Biotechnol.* **30** 715–20
[20] Malheiro A, Morgan F, Baker M, Moroni L and Wieringa P 2020 A three-dimensional biomimetic peripheral nerve model for drug testing and disease modelling *Biomaterials* **257** 120230
[21] Kaewkhaw R, Scutt A M and Haycock J W 2012 Integrated culture and purification of rat Schwann cells from freshly isolated adult tissue *Nat. Protocols* **7** 1996–2004
[22] Hilderink J, Spijker S, Carlotti F, Lange L, Engelse M, van Blitterswijk C, de Koning E, Karperien M and van Apeldoorn A 2015 Controlled aggregation of primary human pancreatic islet cells leads to glucose-responsive pseudoislets comparable to native islets *J. Cell. Mol. Med.* **19** 1836–46
[23] Konings G F J, Cornel K M C, Xanthoulea S, Delvoux B and Skowron M A 2018 Blocking 17 beta-hydroxysteroid dehydrogenase type 1 in endometrial cancer: a potential novel endocrine therapeutic approach *J. Pathol.* **244** 203–14
[24] Püspöki Z, Storath M, Sage D and Unser M 2016 Transforms and operators for directional bioimage analysis: a survey *Focus Bio-Image Inf.* **219** 69–93
[25] Longair M H, Baker D A and Armstrong J D 2011 Simple neurite tracer: open source software for reconstruction, visualization and analysis of neuronal processes *Bioinformatics* **27** 2453–4
[26] Goebbels S *et al* 2010 Elevated phosphatidylinositol 3,4,5-trisphosphate in glia triggers cell-autonomous membrane wrapping and myelination *J. Neurosci.* **30** 8953–64
[27] Huang M, Marchetti L, Parlanti P, Landi S, Tonazzini I, Cecchini M, Piazza V and Gemmi M 2016 Generating trunk neural crest from human pluripotent stem cells *Sci. Rep.* **6** 1–9
[28] Seabrook G R *et al* 2002 Functional properties of the high-affinity TRPV1 (VR1) vanilloid receptor antagonist (4-hydroxy-5-iodo-3- methoxyphenylacetate ester) iodo-resiniferatoxin *J. Pharmacol. Exp. Ther.* **303** 1052–60
[29] Anand P and Bley K 2011 Topical capsaicin for pain management: therapeutic potential and mechanisms of action of the new high-concentration capsaicin 8 patch *Br. J. Anaesth.* **107** 490–502
[30] Willingham K D L, Yoo D Y, Lee K-Y, Im W, Kim M, Choi J H, Youn H-Y, Kim S H, Hwang I K and Chung J-Y 2016 Development of a central nervous system axonal myelination assay for high throughput screening *BMC Neurosci.* **17** 1–13
[31] Ramirez M A and Borja N L 2008 Epalrestat: an aldose reductase inhibitor for the treatment of diabetic neuropathy *Pharmacotherapy* **28** 646–55
[32] Malenczyk K, Keimpema E, Piscitelli F, Calvigioni D, Björklund P, Mackie K, Di Marzo V, Hökfelt T G M,

Dobrzyn A and Harkany T 2015 Fetal endocannabinoids orchestrate the organization of pancreatic islet microarchitecture *Proc. Natl Acad. Sci. USA* **112** E6185–194
[33] Hoang D-T, Matsunari H, Nagaya M, Nagashima H, Millis J M, Witkowski P, Periwal V, Hara M and Jo J 2014 A conserved rule for pancreatic islet organization *PLoS One* **9** 1–9
[34] Barré-Sinoussi F and Montagutelli X 2015 Animal models are essential to biological research: issues and perspectives *Future Sci.* **1** 4–6
[35] Zhang B and Radisic M 2017 Organ-on-a-chip devices advance to market *Lab Chip* **17** 2395–420
[36] Haberberger R V, Barry C, Dominguez N and Matusica D 2019 Human dorsal root ganglia *Front. Cell. Neurosci.* **13** 1–17
[37] Guimarães M Z P *et al* 2018 Generation of iPSC-derived human peripheral sensory neurons releasing substance P elicited by TRPV1 agonists *Front. Mol. Neurosci.* **11** 1–17
[38] Yiangou L *et al* 2019 Method to synchronize cell cycle of human pluripotent stem cells without affecting their fundamental characteristics *Stem Cell Rep.* **12** 165–79
[39] Nestor M W *et al* 2014 A time course analysis of the electrophysiological properties of neurons differentiated from human induced pluripotent stem cells (iPSCs) *PLoS One* **9** 1–14
[40] Meents J E *et al* 2019 The role of Nav1.7 in human nociceptors: insights from human induced pluripotent stem cell-derived sensory neurons of erythromelalgia patients *Pain* **160** 1327–41
[41] Olah Z, Szabo T, Karai L, Hough C, Fields R D, Caudle R M, Blumberg P M and Iadarola M J 2001 Ligand-induced dynamic membrane changes and cell deletion conferred by vanilloid receptor 1 * *J. Biol. Chem.* **276** 11021–30
[42] Gomez-Sanchez J A, Pilch K S, van der Lans M, Fazal S V, Benito C, Wagstaff L J, Mirsky R and Jessen K R 2017 After nerve injury, lineage tracing shows that myelin and Remak Schwann cells elongate extensively and branch to form repair Schwann cells, which shorten radically on remyelination *J. Neurosci.* **37** 9086–99
[43] Gonzalez-Perez F, Udina E and Navarro X 2013 Extracellular matrix components in peripheral nerve regeneration *Int. Rev. Neurobiol.* **108** 1943–8
[44] Hughes C S, Postovit L M and Lajoie G A 2010 Matrigel: a complex protein mixture required for optimal growth of cell culture *Proteomics* **10** 1886–90
[45] Hyung S, Lee S-R, Kim J, Kim Y, Kim S, Kim H N and Jeon N L 2021 A 3D disease and regeneration model of peripheral nervous system–on–a–chip *Sci. Adv.* **7** 1–12
[46] Sternberg J and Kimber S J 1986 Distribution of fibronectin, laminin and entactin in the environment of migrating neural crest cells in early mouse embryos *J. Embryol. Exp. Morphol.* **91** 267–82
[47] Yi J J, Barnes A P, Hand R, Polleux F and Ehlers M D 2010 TGF-β signaling specifies axons during brain development *Cell* **142** 144–57
[48] Du J *et al* 2017 Prompt peripheral nerve regeneration induced by a hierarchically aligned fibrin nanofiber hydrogel *Acta Biomater.* **55** 296–309
[49] Gnavi S, Fornasari B E, Tonda-turo C and Laurano R 2015 The effect of electrospun gelatin fibers alignment on Schwann cell and axon behavior and organization in the perspective of artificial nerve design *Int. J. Mol. Sci.* **16** 12925–42
[50] Daud M F B, Pawar K C, Claeyssens F, Ryan A J and Haycock J W 2012 An aligned 3D neuronal-glial co-culture model for peripheral nerve studies *Biomaterials* **33** 5901–13
[51] Farrukh A, Zhao S and Campo A 2018 Microenvironments designed to support growth and function of neuronal cells *Frontiers in Materials* **5** 1–22
[52] Santos D, Wieringa P, Moroni L, Navarro X and Valle J D 2017 PEOT/PBT guides enhance nerve regeneration in long gap defects *Adv. Healthcare Mater.* **6** 1600298
[53] Gonçalves N P, Vægter C B, Andersen H, Østergaard L, Calcutt N A and Jensen T S 2017 Schwann cell interactions with axons and microvessels in diabetic neuropathy *Nat. Rev. Neurol.* **13** 135–47
[54] Vægter C B 2018 Peripheral glial cells in the development of diabetic neuropathy *Front. Neurol.* **9** 1–9
[55] Cermenati G *et al* 2012 Diabetes-induced myelin abnormalities are associated with an altered lipid pattern: protective effects of LXR activation *J. Lipid Res.* **53** 300–10
[56] Wang-Fischer Y and Garyantes T 2018 Improving the reliability and utility of streptozotocin-induced rat diabetic model *J. Diabetes Res.* **2018** 1–14
[57] Lim H, Sharoukhov D, Kassim I, Zhang Y, Salzer J L and Melendez-Vasquez C V 2014 Label-free imaging of Schwann cell myelination by third harmonic generation microscopy *Proc. Natl Acad. Sci. USA* **111** 18025–30
[58] Wood M D, MacEwan M R, French A R, Moore A M, Hunter D A, Mackinnon S E, Moran D W, Borschel G H and Sakiyama-Elbert S E 2010 Fibrin matrices with affinity-based delivery systems and neurotrophic factors promote functional nerve regeneration *Biotechnol. Bioeng.* **106** 970–9
[59] Belkas J S, Shoichet M S, Midha R and Frcs C 2004 Axonal guidance channels in peripheral nerve regeneration *Oper. Tech. Orthop.* **14** 190–8
[60] Kitsukawa T, Shimizu M, Sanbo M, Hirata T, Taniguchi M, Bekku Y, Yagi T and Fujisawa H 1997 Neuropilin-semaphorin III/D-mediated chemorepulsive signals play a crucial role in peripheral nerve projection in mice *Neuron* **19** 995–1005
[61] Plachez C and Richards L J 2005 Mechanisms of axon guidance in the developing nervous system *Curr. Top. Dev. Biol.* **69** 267–346
[62] Pagan-diaz G J, Ramos-Cruz K P, Sam R, Kandel M E, Aydin O, Saif M T A, Popescu G and Bashir R 2019 Engineering geometrical 3-dimensional untethered *in vitro* neural tissue mimic *Proc. Natl Acad. Sci. USA* **116** 25932–40
[63] Morotti M, Vincent K, Brawn J, Zondervan K T and Becker C M 2014 Peripheral changes in endometriosis-associated pain *Hum. Reprod. Update* **20** 717–36
[64] Morotti M, Vincent K and Becker C M 2017 Mechanisms of pain in endometriosis *Eur. J. Obstet. Gynecol.* **209** 8–13